Statistics of microstructure patchiness in a stratified lake

J. Planella Morato,[1] E. Roget,[1] and I. Lozovatsky[2]

[1]   Statistics of microstructure patches in a sheared, strongly stratified metalimnion of Lake Banyoles (Catalonia, Spain), which occupied ~40% of the total lake depth of 12 m, are analyzed. Light winds (<3 m s^{-1}) dominated the periods of observation in late June and early July of 2009. The patch sizes h_p and the corresponding patch Thorpe scales L_{Tp} were identified using profiling measurements of temperature microstructure and small-scale shear. The distribution of h_p was found to be lognormal with mean and median values of 0.69 m and 0.50 m respectively. The distribution of L_{Tp} within the patches was also fitted to a lognormal model and the mean and median values found to be close to 0.1 m. The probability distribution of the ratio L_{Tp}/h_p was approximated by the Weibull probability model with a shape parameter $c_w \approx 2$, and also by beta probability distribution. For $h_p > 0.25$ m, the ratio L_{Tp}/h_p depends on the patch Richardson and mixing Reynolds numbers following the parameterization of Lozovatsky and Fernando (2002). Analysis of the dynamics of mixing reveals that averaged vertical diffusivities ranged between ~1 × 10^{-4} m^2 s^{-1} and ~5 × 10^{-5} m^2 s^{-1}, depending on the phase of the internal waves. Episodic wind gusts (wind speed above 6 m s^{-1}) transfer ~1.6% of the wind energy to the metalimnion and ~0.7% to the hypolimnion, generating large microstructure patches with h_p of several meters.

1.   Introduction

[2]   Studies of meso and small-scale dynamics in enclosed aquatic basins have shown that wind generates mixing in the surface layer [*Wüest et al.*, 2000] and energizes basin-scale surface and internal seiches [*Imberger*, 1998] that can be traced in lakes for hours and even days after the wind ceases [*Münnich et al.*, 1992; *Roget et al.*, 1997; *Wang et al.*, 2000]. However, small and medium lakes are exposed to low winds most of the time [*Kocsis et al.*, 1998; *Wüest et al.*, 2000; *Gale et al.*, 2006] so, although studies of mixing under a low wind regime are rare they are very important for lakes. Recently, the importance of ocean dynamics under low winds has also been stated [*Hood et al.*, 2010]. Wind gusts can generate intense but short-lived turbulence in inner stratified layers [*Lozovatsky et al.*, 2005], which influences various physical and biochemical processes occurring in lakes [*Ledwell and Bratkovich*, 1995; *Wüest et al.*, 2000; *Evans et al.*, 2008].

[3]   Turbulent events in the thermocline are mostly triggered by shear instabilities [*Smyth et al.*, 2001; *Staquet and Bouruet-Aubertot*, 2001] and internal wave breaking [*Bryson and Ragotzkie*, 1960; *Nishri et al.*, 2000; *Etemad-Shahidi and Imberger*, 2006]. Turbulence produced by shear instability in stratified layers is usually intermittent and often not very energetic [*Imberger and Patterson*, 1990; *Gibson*, 1991b]. In layers close to the lake floor, turbulence is mainly maintained by bottom friction [*D'Asaro and Dairiki*, 1997] although other processes, such as convective instability [*Moum et al.*, 2004; *Lorke et al.*, 2005; *Sanchez and Roget*, 2007] or critical wave reflection [*Slinn and Riley*, 1996; *McPhee-Shaw and Kunze*, 2002; *Puig et al.*, 2004], can also be important sources of turbulence.

[4]   Turbulence not only enhances the transfer of energy, heat, mass, nutrients, suspended particles, oxygen, etc., but also influences other ecosystem processes such as the encounter rate of small-sized predators and their prey [*Rothschild and Osborn*, 1988; *Delaney*, 2003; *Rhodes and Reynolds*, 2007], ingestion rates [*Muelbert et al.*, 1994; *Shimeta et al.*, 1995; *Saiz et al.*, 2003], particle aggregation and disaggregation [*MacIntyre et al.*, 1995; *O'Brien et al.*, 2004; *Jago et al.*, 2006], small-scale patchiness of nutrients [*Brandl et al.*, 1993; *Seuront et al.*, 2001; *Schernewski et al.*, 2005], and growth of species [*Sullivan and Swift*, 2003; *Peters et al.*, 2006].

[5]   To better understand and model the flux paths of physical and biochemical parameters occurring in natural aquatic systems, it is important to know about turbulent scales and intermittency or patchiness characteristics [*Lewis et al.*, 1984; *Peters and Marrasé*, 2000; *Smaoui et al.*, 2007]. Patches can be characterized by the patch size, h_p, and the Thorpe L_{Tp} scales [*Thorpe*, 1977] inside the patches.

---

[1]Department of Physics, University of Girona, Girona, Spain.
[2]Environmental Fluid Dynamics Laboratories, Department of Civil Engineering and Geological Sciences, University of Notre Dame, Notre Dame, Indiana, USA.
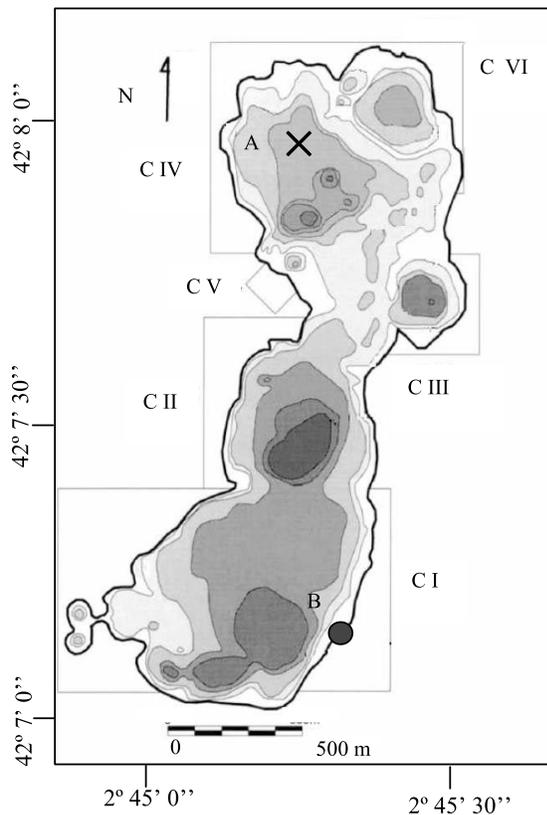
Figure 1. Bathymetric map of Lake Banyoles [from *Moreno-Amich and Garcia-Berthou*, 1989]. With kind permission from Spring Science+Business Media. Distance between the isobaths is 5 m. The main basins (C-I to C-VI) are shown on the map. Point A indicates the measurement site and point B the location of the meteorological station.

The Thorpe scale is assumed to specify the characteristic size of turbulent overturns and can be used as a characteristic turbulent scale to estimate diapycnal diffusivities [*Ferron et al.*, 1998; *Stansfield et al.*, 2001; *Lee et al.*, 2009].

[6] The ratio L_{Tp}/h_p, which we also call the normalized patch Thorpe scale, has been examined in a series of laboratory experiments [*Itsweire et al.*, 1986; *De Silva and Fernando*, 1992], using numerical simulations [*De Silva et al.*, 1996; *Smyth and Moum*, 2000] and based on field measurements [*Lozovatsky and Erofeev*, 1993; *Moum*, 1996; *Pozdynin*, 2002]. *Smyth et al.* [2001] showed that the value of L_{Tp}/h_p can indicate the age of turbulence in a patch. The general tendency of L_{Tp}/h_p to decrease with time has been reported, suggesting that the turbulence is younger when L_{Tp}/h_p is larger. Parameterization of L_{Tp}/h_p in terms of external (ambient stratification) and internal (diffusivity) parameters [*Lozovatsky and Fernando*, 2002] is helpful for understanding the state of turbulence zones. Approximately constant L_{Tp}/h_p close to 0.3 may indicate young or quasi-stationary turbulence, but this ratio is substantially lower for decaying or fossil [*Gibson*, 1980] turbulence. Estimations of photosynthetic rates require parameterization of the vertical movement of phytoplankton, which is based on turbulent scales and vertical diffusivities [*Lande and Lewis*, 1989; *Yamazaki and Kamykowski*, 1991]. Vertical transport of

nutrients [*MacIntyre and Jellison*, 2001; *Lagadeuc*, 2005] depends on the state of turbulence and the encounter rates between prey and predator in plankton [*Davis et al.*, 1991; *Kiørboe*, 1997]. Modeling of vertical displacements of suspended solid particles relies on knowledge of turbulent scales [*Lazaro and Lasheras*, 1992; *MacIntyre et al.*, 1999].

[7] The majority of studies of turbulent scales and patchiness in deep oceans [*Gregg*, 1980; *Gibson et al.*, 1993; *Lee et al.*, 2009] and in shallow seas and lakes [*Baines*, 2001; *Saggio and Imberger*, 2001; *Wüest and Lorke*, 2003] have employed an equal-distance segmentation of the water column, but some authors [*Lozovatsky et al.*, 1993; *Peters et al.*, 1995; *Piera et al.*, 2002] have focused on turbulence in well-defined, bounded turbulent regions (patches).

[8] In this paper, we analyze microstructure patches in the metalimnion (main thermocline) of Lake Banyoles and estimate effective turbulent diffusivity and associated buoyancy flux caused by intermittent mixing events. The study is based on 373 temperature and small-scale shear profiles obtained from the lake during four days of a field campaign in late June – early July of 2009. The wind speed U_{10} was for the most part less than 3 m s^{-1} with a few short-term wind gusts when $U_{10} > 6$ m s^{-1}. The paper is organized as follows. In Section 2, *Background and Observations*, we describe the background hydrodynamics of Lake Banyoles, the observational site in the lake, and the microstructure measurements carried out using a free-falling microstructure profiler. The methodology used in the data processing, patch identification, and computation of turbulent scales are given in Section 3, *Data Processing*. Characteristics of stratification and microstructure are discussed in Section 4, *Results*. This section focuses mainly on the main thermocline of the lake. We examine the statistics of the patch sizes, Thorpe scales, and the ratio L_{Tp}/h_p within the patches, and lognormal, Weibull, and beta probability models are used to describe the distribution of h_p, L_{Tp} and the normalized patch Thorpe scale, L_{Tp}/h_p. The dependence of L_{Tp}/h_p on the patch Richardson number Ri_p and the patch mixing Reynolds number R_{mp} [*Lozovatsky and Fernando*, 2002] is scrutinized. Next, the vertical diffusivities across the main thermocline and effective buoyancy flux are calculated and the effect of the phase of internal seiches on turbulence generation is analyzed. Final comments are given in Section 5.

2. Background and Observations

2.1. Background Hydrography of the Lake

[9] Lake Banyoles (Figure 1) is a multibasin water body in Catalonia, Spain, (42° 7′ N, 2° 45′ E) with a specific hydrodynamic regime [*Casamitjana and Roget*, 1993; *Casamitjana et al.*, 2006]. The surface of the lake is 172 m above sea level, it covers 1.12 km^2 and the maximum depth is 45 m. In late spring and at the beginning of summer, weakly stratified surface (epilimnion) and bottom (hypolimnion) boundary layers are separated by a wide thermocline (metalimnion), which occupies about one third of the mean depth of the entire lake in the summertime [*Roget et al.*, 1997].

[10] From April to October, mild winds with mean speeds below 2 m s^{-1} are frequently observed over the Lake Banyoles area due to a sea breeze regime (the Mediterranean coast is about 30 km to the southeast). As a response to the breeze forcing, a quasi-stationary internal wavefield is

Table 1. Characteristics of the Field Campaign, Wind Speed U_{10}, Wind Stress τ_{10}, and Microstructure Patches

Session	Duration (h)	Number of Profiles	$\langle U_{10} \rangle$ (m s^{-1})	$rms(U_{10})$ (m s^{-1})	$U_{\max}$ (m s^{-1})	$\tau_{10} \times 10^{-3}$ (N m^{-2})	Patches Detected	Patches Accepted	Patches With $h_p > 25$ cm
23 Jun 2009	1.71	81	0.77	0.42	4.03	0.94	659	373	196
25 Jun 2009	2.07	102	3.20	3.20	13.90	12.53	1005	448	326
27 Jun 2009	1.72	98	<0.50	no data	1.30	< 0.37	774	450	323
1 Jul 2009	1.80	92	0.60	2.20	4.47	0.54	880	512	283

established in the thermocline with wave amplitudes of about one meter or even higher [*Roget et al.*, 1993]. Internal waves influence vertical mixing and play an important role in transferring energy to the hypolimnion [*Imberger*, 1994], thereby influencing the transport of biological and chemical patterns (plankton, suspended sediments and nutrients among others), which are sensitive to small scale patchiness [*Garcia-Gil et al.*, 1988].

[11] Internal seiches in lakes are often dominated by high vertical modes [*Perez-Losada et al.*, 2003]. This is the case with Lake Banyoles, where a dominant second vertical first horizontal mode is easily excited [*Roget et al.*, 1997]. The modeling results correlate well with historical data collected in Lake Banyoles, which are applied to the field data and discussed in Section 4.

2.2. Measurements and Instrumentation

[12] The measurements were conducted during four days in June–July 2009 (see Table 1) at a gently sloping site in the western part of the northern lobe of the lake (the C-IV basin in Figure 1). The test site (~12 m depth) was exposed to a southeasterly breeze with a fetch of ~2 km. The lake is surrounded by hills on all sides except the southeast, where a plain extends toward the Mediterranean Sea. The wind was measured at a meteorological station (Davis Vantage Pro 6150C) located 1 km to the southeast of the test site (Figure 1). The wind speed and wind direction were averaged over 30-min periods. The atmospheric forcing over the lake during the period of the observations was dominated by northwesterly and southeasterly winds up to ~3 m s^{-1}. Irregular wind gusts (with U_{10} up to 6–15 m s^{-1}) originated episodically over the lake due to uneven heating of the lake surface and surrounding mountains, lasting only a few minutes. The wind stress, τ_{10}, was calculated using the bulk formulas for light winds [*Wu*, 1994] and 30-min averaged wind speed $\langle U_{10} \rangle$. Under light winds (<1 m s^{-1}), τ_{10} was less than 10^{-3} N m^{-2} increasing by an order of magnitude when the wind rose to about 3 m s^{-1}.

[13] The profiling measurements in the lake started every day as soon as the breeze reached the test site (usually about 2 P.M.). We used the Sea and Sun Microstructure Turbulence system (MSS) [*Prandke and Stips*, 1998] at a sinking speed 0.85 m s^{-1}. The profiler was equipped with microstructure temperature and shear sensors. It had a fast thermistor (FP07) with a sensitivity of 0.001°C and time response of 7 ms, leading to a vertical resolution of 0.6 cm. The resolution of the small-scale airfoil shear probe was 2 cm [*Prandke et al.*, 2000]. The profiler also carried a standard conductivity, temperature, and depth (CTD) package (a thermistor with a sensitivity of 0.001°C and a time response of 160 ms, a conductivity cell with a sensitivity of 0.001 mS m s^{-1} and a time response of 100 ms, and a pressure gauge with a sensitivity of 100 Pa and a time

response of 30 ms). Vertical resolution of the CTD profiles was ~14 cm after data processing (see Section 3.1).

[14] The individual casts were launched from the lake surface to the very bottom of the lake approximately every two minutes for ~2 h. Basic information about the measurements is given in Table 1. The total number of profiles is 373. Standard conditioning of the measurements followed *Roget et al.* [2006]. Reliable data were obtained from 2 m below the lake surface down to about 0.5 m from the bottom.

3. Data Processing

3.1. CTD Data

[15] An exponential recursive filter [*Middleton and Foster*, 1980; *Fozdar et al.*, 1985; *Lueck and Picklo*, 1990] was applied to the conductivity signal to minimize spikes in salinity and density profiles caused by different time responses of the temperature and conductivity sensors. Potential density was calculated based on the UNESCO routines [*Chen-Tung and Millero*, 1986]. The equation of state for fresh water [*Fofonoff and Millard*, 1983; *Chen-Tung and Millero*, 1986] was used, taking into account the concentration of suspended solids [*Sanchez and Roget*, 2007].

[16] Since vertical resolution of the CTD profiles was 14 cm at best, we averaged temperature (T) and potential density (ρ_s) to acquire a standard vertical resolution $\Delta z = 0.2$ m with which to analyze background stratification. The buoyancy frequency $N^2 = \frac{g}{\rho_s} \frac{\Delta \rho_s}{\Delta z}$, where g is gravity, was calculated using sorted density profiles ρ_s [*Thorpe*, 1977].

3.2. Microstructure Data

3.2.1. Patch Identification and Calculation of the Thorpe Scale

[17] The identification of microstructure patches was based on individual Thorpe displacement profiles $d'_T(z)$, which are the vertical distances that fluid particles need to be moved to obtain a stable monotonous density profile, assuming that density inversions are caused by vertical mixing. The Thorpe scale, L_T [*Thorpe*, 1977], is defined as the root mean square of Thorpe displacements inside a turbulent region (patch) or at a fixed segment

$$L_T = \left\langle \left(d'_T(z) \right)^2 \right\rangle^{\frac{1}{2}}, \qquad (1)$$

where angular brackets denote ensemble averaging. The Thorpe scales must be calculated based on high-resolution density measurements. Since density in fresh water is almost completely determined by temperature, temperature profiles are commonly used to compute L_T in lakes [*Thorpe*, 1977; *Lorke and Wüest*, 2002; *Roget et al.*, 2006]. To avoid false displacements resulting from noise, temperature profiles were first averaged over $\Delta = 0.8$ cm. This averaging also
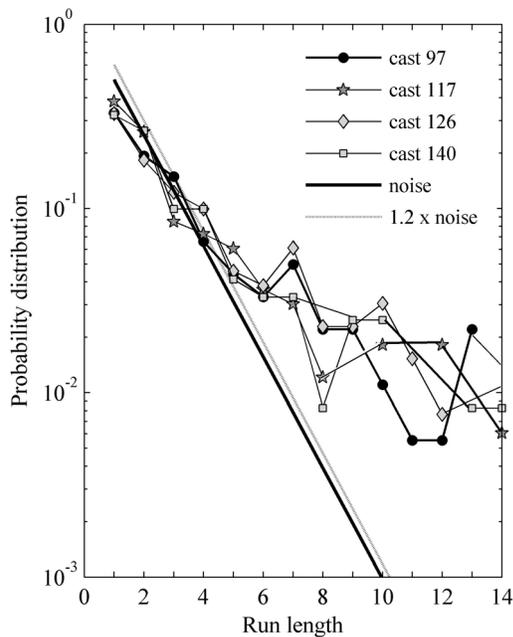
Figure 2. The probability density functions of the Thorpe run lengths for different profiles. The pdfs of random, uncorrelated noise (thick line) and of the noise factor 1.2 (dashed line). The intersection between the measured and noise pdfs indicates the cutoff run length equals 5.

eliminated scales that could not be resolved due to the time response of the temperature sensor. The microstructure patches were then identified automatically as segments with nonzero $d'_T(z)$, providing that the distance between them was larger than 6 cm. This criterion was based on our preliminary visual inspection of numerous pairs of small-scale shear $u'_z(z)$ and $d'_T(z)$ profiles. If the distances between consecutive d'_T segments were less than 6 cm, these segments were combined into one patch. The algorithm, however, considers not only the nominal accuracy of the sensors but also takes into account the actual noise level of the signal [*Thorpe*, 1977]. We implemented a statistical run-length test, the so-called Galbraith Kelley (GK) test [*Galbraith and Kelley*, 1996] to differentiate turbulent patches and noise segments. A 'run' was defined as the number of points (n) with consecutive positive values of $d'_T(z)$ in the patch. If patches are generated by uncorrelated random series of displacements, the probability of observing n positive and negative values must be the same. Hence, the probability density function (pdf) of the run length of a random variable n is [*Larsen and Marx*, 1986]

$$P(n) = 2^{-n}. \tag{2}$$

The pdf of d'_T would be expected to follow equation (2), if noise were a source of inversions in temperature profiles. The GK test identifies a minimal acceptable run length as the point where the experimental pdf of the run lengths intersects the pdf of the noise (equation (2)). Following *Galbraith and Kelley* [1996], we added the root mean square of the run lengths of series r to equation (2) in order to

accept a patch. For an uncorrelated random series, $r = 2.45$ [*Timmermans et al.*, 2003].

[18] To specify a safety margin, *Johnson and Garrett* [2004] considered a scaled amplitude Q of the noise

$$Q = \frac{\delta T}{\left(\frac{dT}{dz}\right)h_p}, \tag{3}$$

where h_p is the patch height, δT the resolution of the temperature sensor and $\frac{dT}{dz}$ the background temperature gradient computed using the reordered temperature profile. Taking density profiles with added random and uncorrelated noise, *Johnson and Garrett* [2004] plotted r for $d'_T(z)$ as a function of Q and n (hereafter referred as JG plots). Once the Q and n parameters of a set of experimental data are found, the JG plots can be used to assess the noise threshold for the measured displacements.

[19] The non-dimensional parameter Q was calculated and plotted as a function of n (not shown here) and compared with the JG plots. The maximum r appeared to be 1.2, which is the factor to be added to the cut-off value. The result of the run-length test is given in Figure 2, which shows $n = 5$ as an estimate of the cut-off run length. Thus, the $d'_T(z)$ with $h_p < 5\Delta = 4$ cm segments were not accepted as microstructure patches.

[20] The resolution of the microstructure temperature sensor, $\delta T \sim 0.001°C$, imposed an additional constraint on the smallest sizes of detectable patches based on the value of the Thorpe scale within the patch [*Galbraith and Kelley*, 1996]

$$L_{Tp\,\min} = 2\frac{g\alpha\delta T}{N^2}, \tag{4}$$

where α is the thermal expansion coefficient.

[21] For N^2 in the range $5 \times (10^{-3} - 10^{-5})$ s^{-2}, $L_{Tp\min}$ varies between ~1 and 7 cm. Combining the constraints imposed by vertical and temperature resolutions, we used an intermediate condition for patch detection [*Lee et al.*, 2009]. As a result, no segments with $h_p > 4$ cm and $L_{Tp} < 4$ cm were considered as turbulent patches.

[22] Table 1 summarizes the results of the displacement analysis including the number of detected and accepted patches and the number of patches with $h_p > 25$ cm, which were used to estimate the mean kinetic energy dissipation rate from a small scale shear within the patch height.

3.2.2. Calculation of the Dissipation Rate and the Buoyancy Reynolds Number

[23] The turbulent kinetic energy (TKE) dissipation rate, ε, was estimated by fitting the empirical spectral densities of a small-scale shear signal to an analytical form of the transversal *Panchev and Kesich* [1969] shear spectrum [see *Roget et al.*, 2006]. The dissipation in patches was identified well by the airfoil sensor [*Wüest et al.*, 1996; *Kocsis et al.*, 1999], ranging between 10^{-4} and 10^{-9} W kg^{-1}.

[24] We also calculated the patch buoyancy Reynolds number, $Re_b = \varepsilon/\nu N^2$, in order to evaluate turbulence activity in stratified layers. *Gibson* [1991a] argued that turbulence is active when $Re_b > 30$. *Rohr et al.* [1984] suggested critical $Re_b = 10 - 16$, which is in agreement with direct numerical simulations of homogeneous turbulence in stratified shear flows [*Itsweire et al.*, 1993]. Analyzing data obtained in
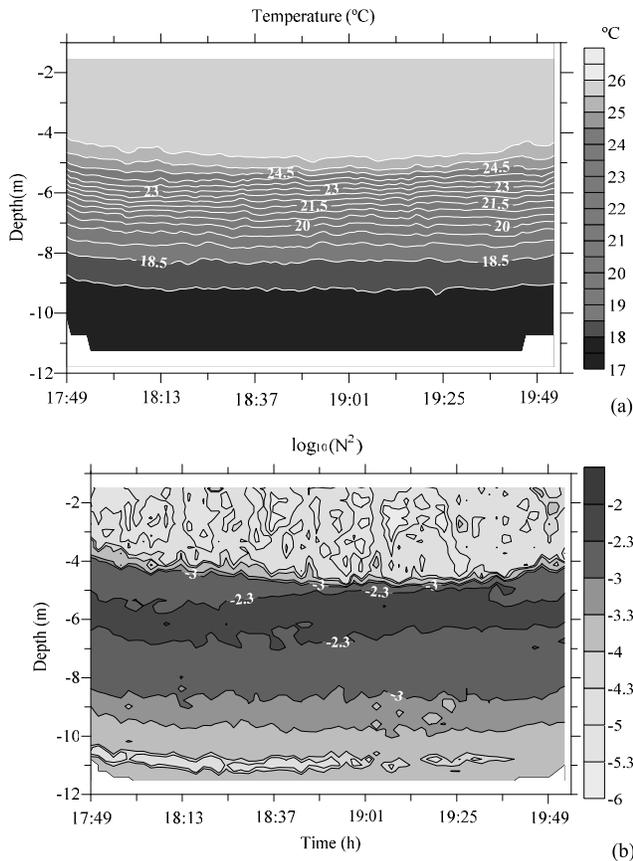
Figure 3. The contour plot of (a) temperature T and (b) logarithm of squared buoyancy frequency $\log_{10}N^2$ for June 25 (N is in s^{-2}).

Knight Inlet (Vancouver, Canada), *Gargett et al.* [1984] proposed a wide range of critical Re_b of from 18 to 165. *Crawford* [1986] noted that the high critical values of Re_b reported by *Gargett et al.* [1984] correspond to very active turbulent regions that are less influenced by regular internal waves but are associated with topographic lee waves accompanied by shear instabilities.

4. Results

4.1. Basic Characteristics of Stratification, Internal Seiches, and Turbulence

[25] The temperature, $T(z,t)$, and squared buoyancy frequency, $N^2(z,t)$, contour plots are shown in Figure 3 for the measurements taken under moderate winds (June 25), and in Figure 4 and Figure 5 under light winds (June 27 and July 1 respectively). The contour plots of the dissipation rate $\varepsilon(z,t)$ computed for segments of 0.5 m for the same period are presented in Figure 6, together with the locations of turbulent patches with $h_p > 25$ cm (see Table 1). It appears that the different patterns of the dissipation field generally correlate well with the locations and sizes of the microstructure patches. Based on the plots shown in Figures 3–6, three major layers of the water column were specified.

[26] We consider the epilimnion, or surface layer (SL), as the layer between the lake surface and the depth where N^2 sharply exceeds 10^{-3} s^{-2}. This layer was directly influenced by wind stress and heat fluxes. The depth of this layer varied between 2.5 and 4.5 m depending on the atmospheric forcing prior to and during the observational periods. Stratification in the SL increased ($N^2 > 10^{-4}$) during periods of low winds ($U_{10} < 0.5$ m s^{-1} on June 27 and July 1). Sustained wind-induced turbulence in the SL is characterized by $\varepsilon > 10^{-8}$ W kg^{-1}.

[27] The metalimnion, or main thermocline (MT), starts immediately below the SL. It was strongly stratified (with a highest mean of $N^2 \sim 10^{-2}$ s^{-2}) and its thickness varied between 4 and 6 m in the depth range below the SL, with $z \sim 8.5$ m occupying $\sim$35–55% of the water column. Turbulence was patchy (Figure 6), with several episodes of large overturns.

[28] Internal waves in the thermocline are easily recognizable in Figure 5a. The opposite direction of the vertical displacements of the upper and lower boundaries of the thermocline (Figure 5a, dashed lines) points to a dominant second mode of internal seiche. The expected horizontal displacements in each layer are shown in Figure 5 by white arrows. A two-dimensional three-layered hydrodynamic model [*Münnich et al.*, 1992] was used to simulate the dynamics of internal seiches in the lake for stratification observed on July 1. It was found that the period of the second vertical first horizontal internal mode (V2H1) was
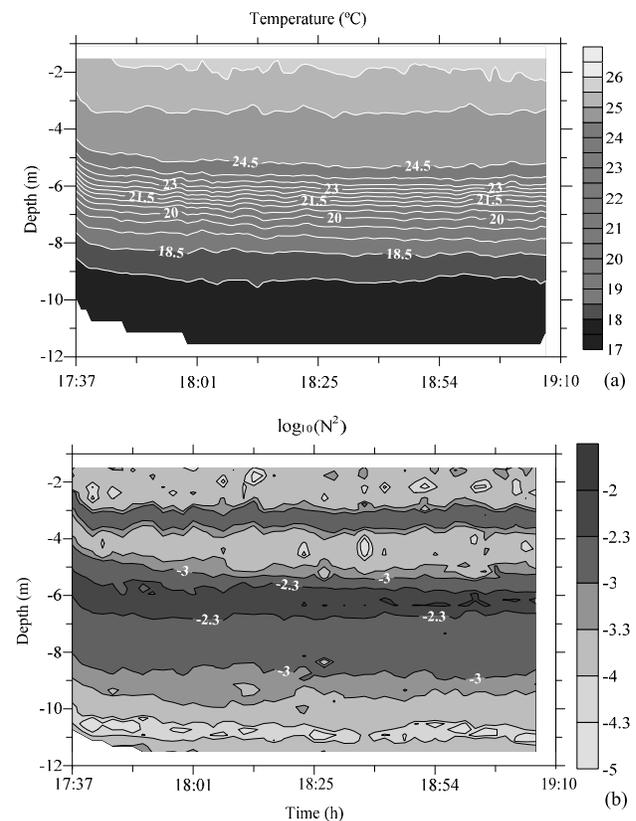
Figure 4. The contour plot of (a) temperature and (b) $\log_{10} N^2$ for June 27.
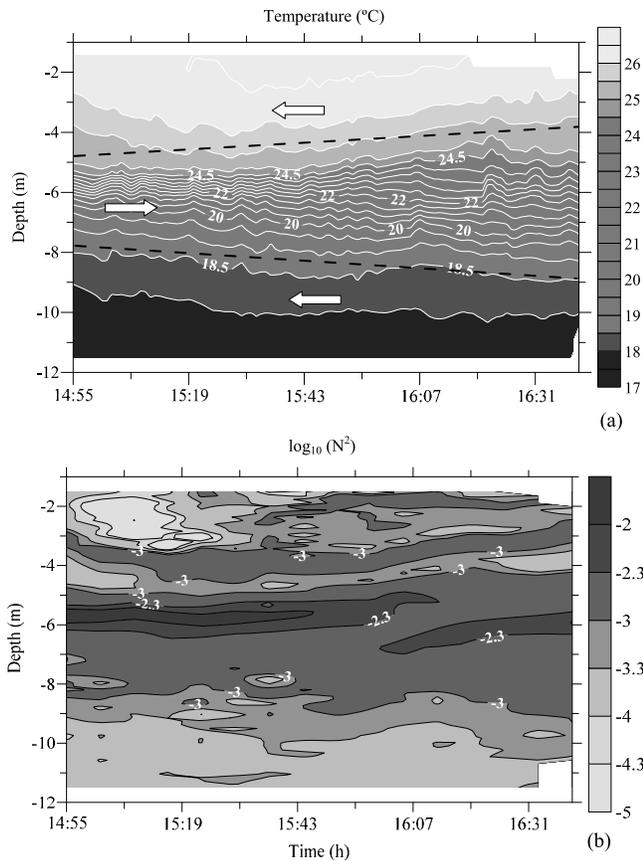
Temperature (°C)

$\log_{10}(N^2)$

Figure 5. The contour plot of (a) temperature and (b) $\log_{10} N^2$ for July 1. The opposite slopes of the upper and lower boundaries of the thermocline marked by dashed lines point to the dominant second mode of the internal seiche. The directions of flow in each layer are shown in Figure 5a by white arrows.

about 12 h, which is in agreement with the results obtained previously for similar atmospheric conditions and stratification in the lake [*Roget et al.*, 1997]. Field measurements on June 25 and 27 started two hours later than on July 1 and were therefore affected by a different phase shift in the V2H1 seiche mode, which follows from the time evolution of the isotherm depths shown in Figures 3 and 4.

[29] To obtain a clearer view of the vertical structure of the horizontal velocity in the MT, we calculated the normal modes for a characteristic $N^2(z)$ profile shown in Figure 7b using a discretized version of the Taylor-Goldstein equations (see *Thorpe* [2005] for details). The vertical profile of the horizontal velocity u of the dominant second vertical mode was used to estimate the shear $V_z(z)$ profile of the internal seiche and the corresponding 'seiche Richardson number', $R_i = N^2/V_z^2$ (vertical step $\Delta z = 0.5$ m). Horizontal velocity and Richardson number are shown in Figures 7a and 7c, respectively. Low Ri values are concentrated near the upper and lower boundaries of the MT, where the internal-seiche shear is high (the critical value of $Ri = 0.25$ is marked in Figure 7 by a dashed line). Depending on the seiche phase and mode structure, turbulence in the thermocline can be generated by seiche-induced shear instabil-

ity [*Münnich et al.*, 1992]. Calculation of Ri at 15 min time intervals during the entire period (12 h) of the seiche dominant V2H1 mode allowed simulation of the cumulative distribution function (CDF) of Ri in the thermocline, which is shown in Figure 8. The Richardson number was less than critical for shear-induced turbulence ($Ri < 0.25$) approximately 25% of the time and in about 55% of cases it was below 1. It is important to emphasize that the vertical shear associated with the oppositely directed internal-seiche induced currents can episodically create shear instability in the thermocline and hence generate smaller scale internal waves and turbulent patches.

[30] It should be noted that the MT periodically contained several sub-layers. For example, on June 27 when the wind speed was less than 0.5 m s^{-1} during the entire observational period, the MT ($\Delta z = \sim 2.5$–8.5 m) contained three definitive sub-layers. A 1 m wide diurnal thermocline [*Imberger*, 1985] underlay the SL where $N^2 \approx (1 - 5) \times 10^{-3}$ s^{-2}. Below it, a less stratified inner layer ($N^2 < 10^{-3}$ s^{-2}) was observed down to $z \sim 4.5$ m. Several turbulent patches were detected in this layer; some of them with a high of $\varepsilon \approx 5 \times 10^{-6}$ W kg^{-1}. The most strongly stratified sub-layer ($\Delta z = \sim 4.5$–8.5 m with $N^2 \approx 5 \times 10^{-3}$ s^{-2}) contained microstructure patches, which were generally small and weak. The same sub-layer structure in the MT was found on July 1 when the wind speed was also low (Figure 5b). The depths of the sub-layers varied over time due to the influence of internal waves. In contrast, on June 25, when higher winds preceded the microstructure measurements, the MT did not contain any sub-layers and the SL deepened to $z \sim 4.5$ m.

[31] The hypolimnion, or bottom layer (BL), extended from the base of the MT ($z \sim 8.5$ m) down to the bottom of the lake. The BL thickness was about 3 m with N^2 varying from 10^{-5} to 10^{-3} s^{-2}, and several episodes of relatively strong turbulent events with $\varepsilon \geq 5 \times 10^{-8}$ W kg^{-1} were observed. The rest of the BL was filled with microstructure patches with a relatively low dissipation rate. A thin (~ 1 m wide) temporal weakly stratified ($N^2 < 5 \times 10^{-5}$ s^{-2}) sub-layer was located at $z \sim 10$ m (Figures 3b and 4b). The dissipation rates at this level and shown in Figure 6 suggest that it is not a turbulent region. It is most probably associated with a slow moving intrusion from a remote region of the lake [*Planella et al.*, 2009].

4.2. Wind Gusts and Turbulent Events

[32] Powerful wind gusts lasting several minutes episodically passed over the lake in the late afternoon. They generated highly energetic turbulent regions across almost the entire water column. We were lucky to measure a series of five consecutive casts that embraced one of these events (marked by an arrow in Figure 6a). Its evolution can be analyzed based on the Thorpe displacement $d'_T(z)$ and small scale shear $u'_z(z)$ profiles, which are shown in Figure 9. The event was captured on June 25, when a maximum wind speed of 7.7 m s^{-1} was recorded during the sampling time of the meteorological data. The first cast in this series was taken at 19:00 and shows a weakly turbulent SL 4.5 m in depth. The corresponding Thorpe displacements depict a classic Z-shape segment [*Gibson*, 1987]. The averaged dissipation rate in the SL was relatively low, $\tilde{\varepsilon}_{SL} \approx 2.8 \times 10^{-8}$ W kg^{-1}, and the corresponding buoyancy Reynolds number was $Re_b = \varepsilon/\nu N^2 \approx 900$. No microstructure patches
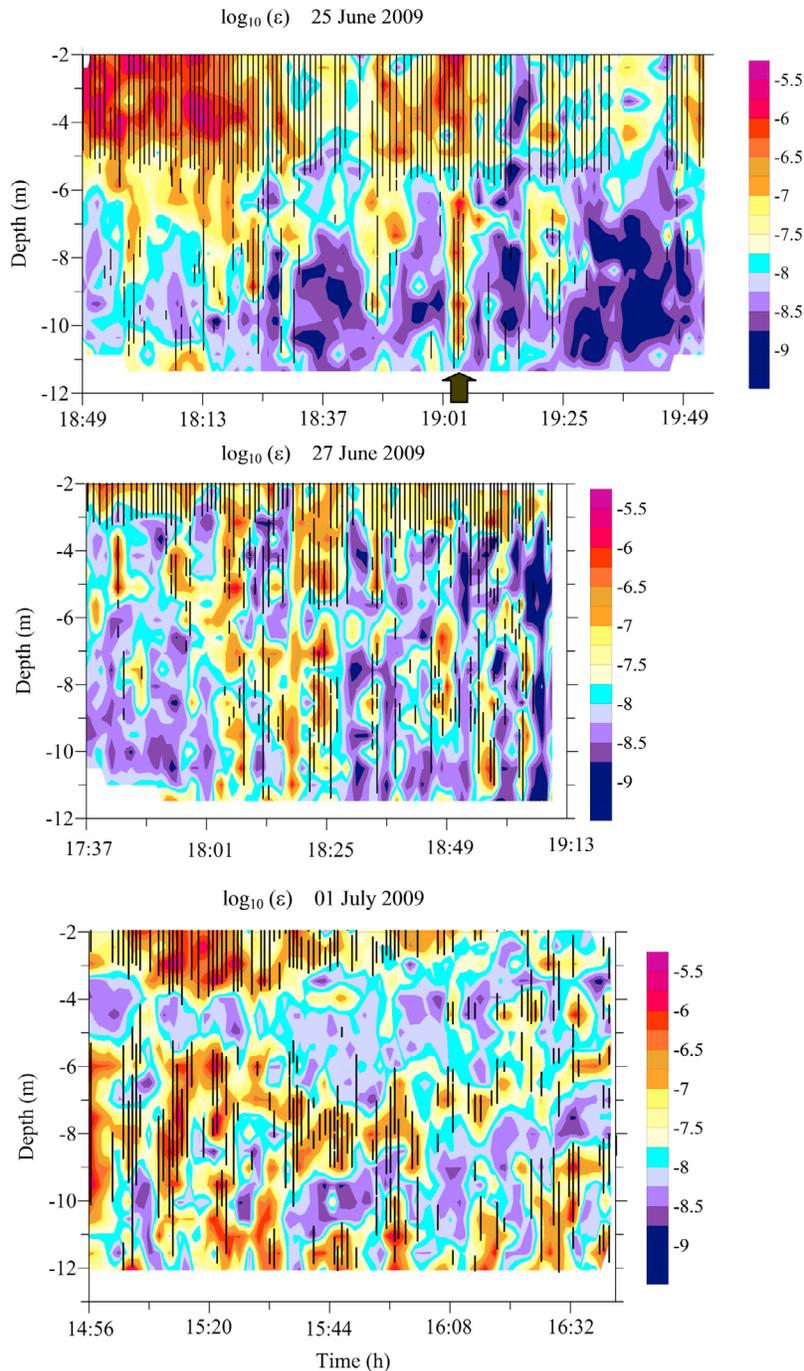
Figure 6. Alignment of microstructure patches (vertical lines) in the background of $\log_{10} \varepsilon$ for (top) June 25, (middle) June 27 and (bottom) July 1. The dissipation rate is in W kg^{-1}. The arrow in Figure 6 (top) points to the turbulent event induced by the wind gust.

were detected in the MT or BL during this cast. The thickness of the SL in the next profile (19:02 h) increased to $z = 5$ m and the averaged dissipation rate went up by about two orders of magnitude, $\tilde{\varepsilon}_{SL} \approx 2.3 \times 10^{-6}$ W kg^{-1} ($Re_b \approx$ 4800). A big new turbulent patch emerged below $z = 6.15$ m, with $\tilde{\varepsilon}_{BP} \approx 1.2 \times 10^{-6}$ W kg^{-1} and $Re_b \approx 900$. The third profile in the series, taken at 19:03:30 h, shows that the thickness of the SL (4.7 m) and $\tilde{\varepsilon}_{SL} \approx 2.2 \times 10^{-6}$ W kg^{-1} was almost the same as during the second cast, but the amplitudes of Thorpe

displacements and the dissipation within the big patch had slightly decreased ($\tilde{\varepsilon}_{BP} \approx 7 \times 10^{-7}$ W kg^{-1} and $Re_b \approx 450$). The following profile taken at 19:05:30 h demonstrates active turbulent mixing in the SL with a mean dissipation of $\tilde{\varepsilon}_{SL} \approx 10^{-6}$ W kg^{-1} ($Re_b \approx 1500$) and a depth increased to ~5.5 m due to the entrainment at the SL base. However, as the wind stress at the surface weakens, several microstructure patches still exist in the MT and BL, with $\tilde{\varepsilon}_{BP} \approx 2 \times 10^{-7}$ W kg^{-1} and $Re_b \approx 300$. One and a half minutes later, at
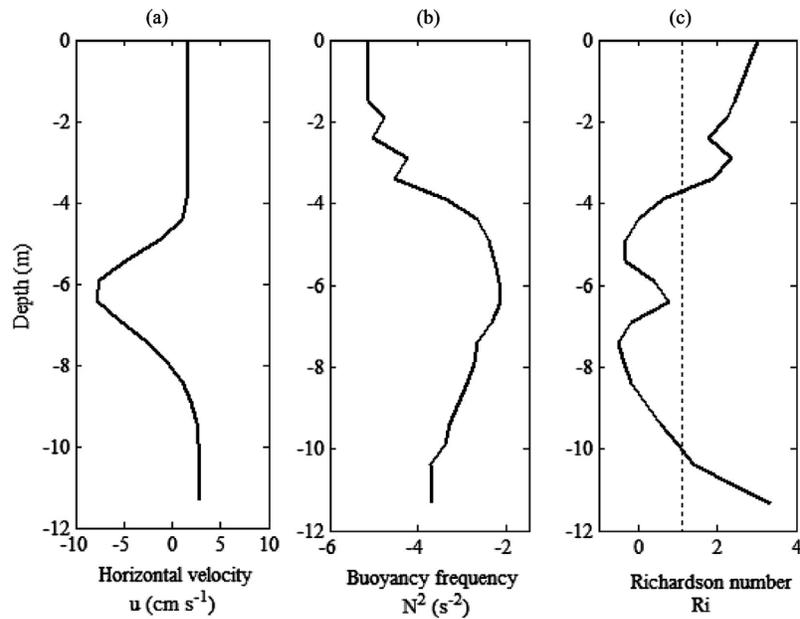
Figure 7. (a) The horizontal velocity profile of the second vertical mode of internal seiche u calculated for (b) a characteristic N^2 profile and (c) the resulting profile of $\log_{10} Ri$.

19:07 h, the fifth cast in the series shows a similar microstructure profile in the SL and no patches in the MT or BL to what was observed in the first cast.

[33] We also analyzed the evolution of turbulence in the surface layer based on the L_{Tp}/h_p ratio, which is supposed to decrease with time as turbulence ceases in a patch [*Smyth et al.*, 2001]. It was found that L_{Tp}/h_p decreased from ~0.2 to ~0.1 between 19:00 h and 19:02 h. During the next three and a half minutes, L_{Tp}/h_p decreased only slightly, remaining close to 0.1. The observed evolution of L_{Tp}/h_p is consistent with direct numerical simulations of a shear-driven overturn as it becomes turbulent [*Smyth et al.*, 2001, Figure 4a].
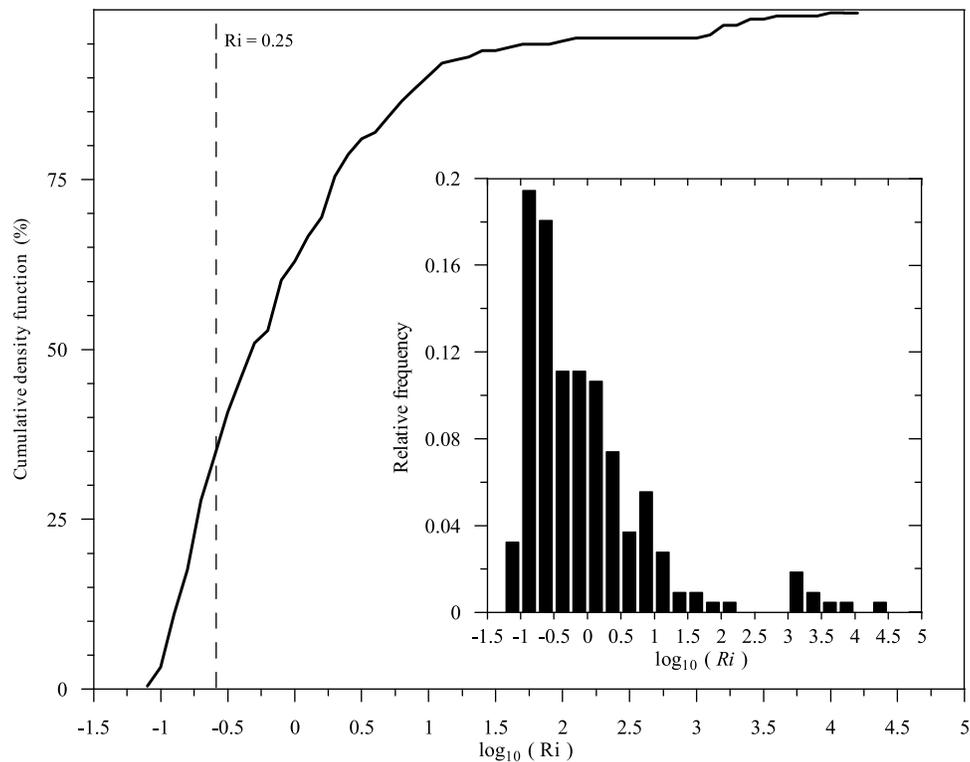
Figure 8. The cumulative distribution function (CDF) of the simulated seiche Richardson numbers Ri in the thermocline. The histogram of Ri is in the insertion.
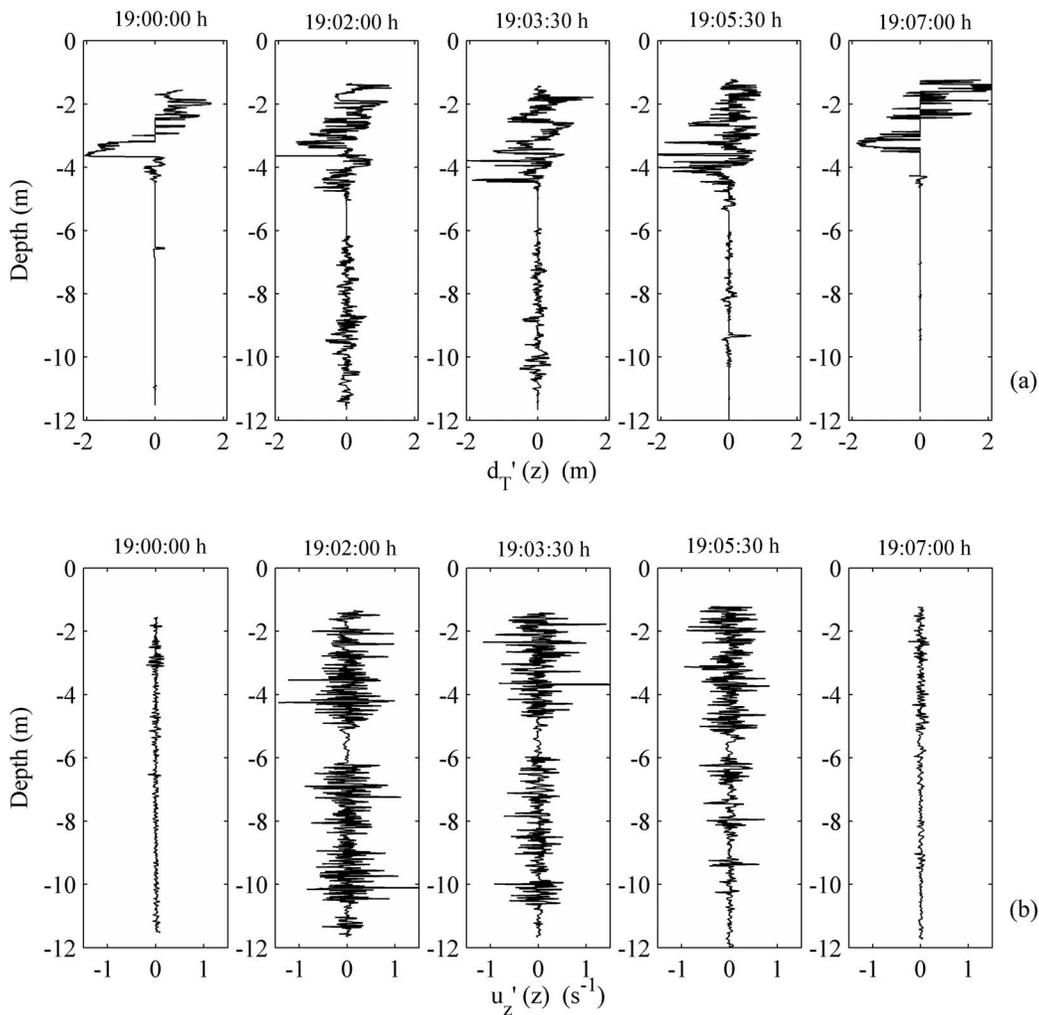
Figure 9. A series of (a) Thorpe displacements $d_T'(z)$ and (b) small-scale shear $u'_z(z)$ profiles taken on June 25 during the passage of a wind gust (see text for details).

[34] To evaluate the impact of wind gusts on internal mixing, the wind energy flux at 10 m above the lake's surface

$$P_{10} = \rho_{air} C_{10}\ U_{10}^3 \qquad (5)$$

was calculated [*Lombardo and Gregg*, 1989], with the air density ρ_{air}, and the drag coefficient C_{10} computed following *Wu* [1994]. For $U_{10} = 7.7$ m s^{-1}, $P_{10} = 0.44$ W m^{-2}.

[35] The integrated dissipation $\tilde{P}$ in a specific layer of the water column (between z_1 and z_2) can be evaluated [*Wüest et al.*, 2000] as

$$\tilde{P} = \int_{z_1}^{z_2} \rho_w \langle \varepsilon \rangle (z)\ dz, \qquad (6)$$

where $\langle \varepsilon \rangle (z)$ is zero for non-turbulent segments and equal to the mean dissipation for each patch within the layer. Since wind gusts directly influenced the second, the third and the fourth profiles shown in Figure 9, we estimated $\tilde{P}$ in the SL, MT and BT by averaging the dissipation rate measured between 19:02:00 h and 19:05:30 h. In the SL, $\tilde{P}_{SL} = 7.1 \times 10^{-3}$ Wm^{-2}, which is about 1.6% of P_{10}. In the lake's interior, $\tilde{P}_{in} = 3.1 \times 10^{-3}$ Wm^{-2}, equal to ~0.7% of P_{10}.

[36] *Wüest et al.* [2000] reported that in Lake Alpnach about 1.5% of the wind energy dissipated in the surface layer and less than 0.7% in the stratified interior of the lake. Much lower values of $\tilde{P}_{SL}$ in lakes [*Wüest and Lorke*, 2003; *Folkard et al.*, 2007] compared to the ocean, where *Lozovatsky et al.* [2005] found $\tilde{P}/P_{10} = 3 - 7\%$ for moderately high winds, are related to wind work lasting a short time during the passage of wind gusts. Transfer of potential energy from wind gusts to the SL and MT can increase the instabilities of the internal wavefield, and pressure fluctuations could also transport energy to the interior of the water.

[37] Rare large turbulent events that are presumably related to wind gusts may represent individual samples from a different statistical population to the main population of regular sheared MT patches. These patches were identified as outliers of the box plot distribution of h_p (not shown here). It was found that the outliers were outside the 2nd and 98th percentile, i.e., $h_p \in [0.10, 3.5]$ m, so we did not use these samples for further analysis. The statistical indepen-
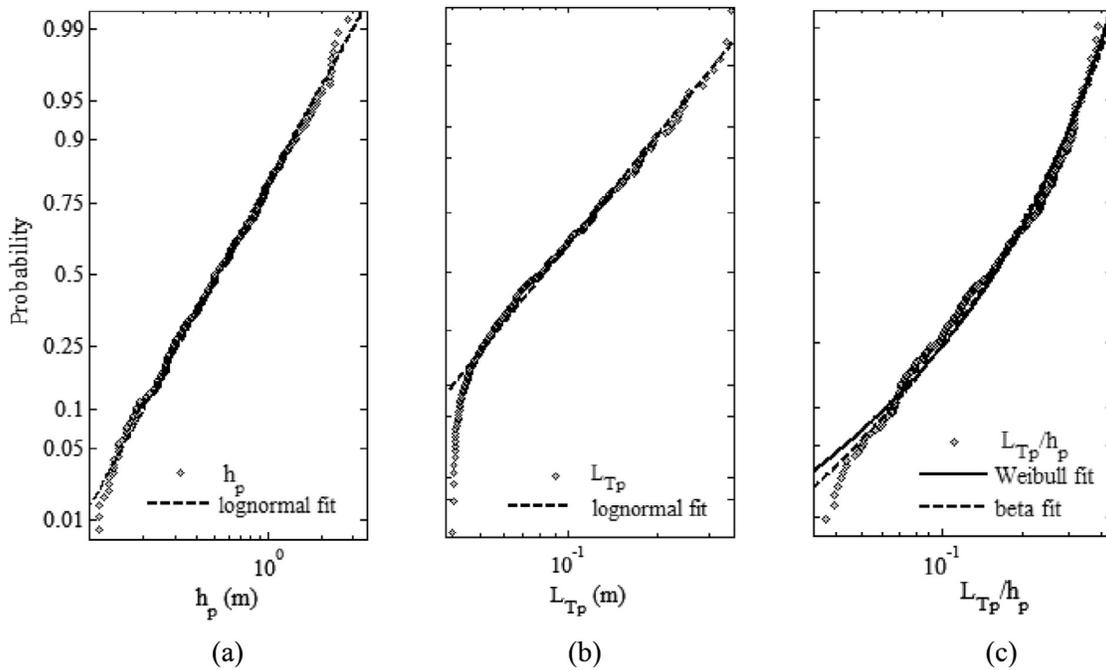
Figure 10. The cumulative distribution functions (CDF) of (a) the patch sizes h_p in the thermocline and (b) the patch Thorpe scale L_{Tp} fitted by lognormal model (dashed lines). (c) The CDF of the normalized patch Thorpe scale L_{Tp}/h_p is approximated by the Weibull (solid line), and beta (dashed line) distributions.

dence of the remaining patches was analyzed for a complete set of the profiles as well as for three subsets containing every second, third, and forth profile. It appears that the complete data set (315 patches) can be considered as a series of statistically independent samples.

4.3. Microstructure Patches, Turbulent Scales, and Diffusivities in the Thermocline

[38] The generation of turbulence in water's interior and boundary layers is usually governed by different processes. In this section, we focus on the main thermocline (meta-limnion) under low winds, and far from the boundaries where turbulence generated by an internal wavefield is usually patchy. The prevailing mechanisms in the SL and BL are wind and bottom stress respectively.

[39] The average thickness of the MT during the campaign was in the range 4 to 6 m. Results of the statistical analysis are presented in the following sections.

4.3.1. Patch Size

[40] The cumulative distribution function (CDF) of the sizes of the microstructure patches h_p detected in the MT is shown in Figure 10a. The total number of patches in the MT that met our selection criteria was 315. Large rare turbulent events detected in the MT, generated mostly by short, powerful wind gusts, were excluded (see Section 4.2).

[41] Figure 10a shows that about 95% of the empirical cumulative distribution function $F(h_p = 0.14 - 2.15 \text{ m})$ can be approximated by lognormal distribution

$$F\left(h_p\right) = \frac{1}{2} erfc\left[-\frac{ln(h_p) - \mu}{\sigma\sqrt{2}}\right], \quad (7)$$

where $erfc$ is the complimentary error function [*Crow and Shimizu*, 1988] and the parameters of the fit $\mu = \langle ln(h_p)\rangle =$

-0.65 ± 0.08 and $\sigma^2_{\mathbf{ln}(h_p)} = 0.75 \pm 0.05$. The corresponding mean and median values are $\langle h_p\rangle = 0.69$ m, $med(h_p) = 0.50$ m. The Kolmogorov-Smirnov test [*Ayyub and McCuen*, 1996] of the goodness of the fit suggests that (7) cannot be rejected as a probability model for the empirical CDF (p-value = 0.89; K-S statistics are 0.032, which is less than the K-S critical value of 0.076 at the 95% confidence level).

[42] Lognormal distribution has been used as an approximation of patch sizes in various regions of ocean and coastal marine waters [*Lozovatsky et al.*, 1993; *Pozdynin*, 2002]. *Stansfield et al.* [2001] reported that the probability distribution of patch sizes in the ocean pycnocline can be considered as lognormal for 70% of their data (1 m < h_p < 15 m). *Yamazaki and Lueck* [1987] in turn suggested Gamma (or a simpler exponential) distribution as a possible approximation of $F(h_p)$. Our analysis of MT patches in Lake Banyoles confirms the lognormality of h_p distribution in the range ~0.14 m < h_p < 2.15 m.

[43] *Lozovatsky and Fernando* [2002] pointed out that the probability distributions of the sizes of turbulent regions as well as other properties of turbulence, such as turbulent scales and patch-averaged dissipation rates, are expected to be lognormal due to the similarity between the breakdown of turbulent eddies and the sizes of particles resulting from a series of successive statistically independent breakdowns, which is considered as asymptotically lognormal [*Kolmogorov*, 1941].

4.3.2. The Thorpe Scale L_{Tp} Within Patches

[44] The probability distribution of the Thorpe scale $F(L_T)$ has been analyzed in different aquatic environments mainly based on equal-distance segmentation of the Thorpe displacement profiles. *Alford and Pinkel* [2000] found that for $L_T \geq 1.5$ m (CTD measurements in the thermocline of the Pacific Ocean) the tails of a lognormal distribution fit the

empirical data well. *Stansfield et al.* [2001] also reported the lognormal model to be an appropriate fit for $F(L_T)$ in the pycnocline of the Juan de Fuca Strait based on CTD measurements. *Kitade et al.* [2003] and L. M. Huzzey and T. M. Powell (Tidal variation in turbulent eddy sizes in an estuary, unpublished manuscript, 2005) showed histograms of L_T that are clearly skewed to high values. The authors stated that the distributions were definitely not normal, but no formal approximation was suggested. All of these results were obtained for L_T larger than 0.4 m. It should be noted that the Thorpe scale in all the publications referred to was calculated at fixed, equally distant segments of the water column. For such a type of L_T data, *Lorke and Wüest* [2002] found exponential rather than lognormal distribution to be the best fit for $F(L_T)$. The measurements were taken in Lakes Baikal (Russia), Neuchâtel (Switzerland), and Müggelsee (Germany). The exponential model can be appropriate for $F(L_T)$ when L_T is calculated at the segments of $d'_T(z)$ profiles with arbitrary (usually equal) length, where the probability of zero L_T is not zero. For microstructure patches, however, the exponential model cannot be applied because $F(L_{Tp} = 0)$ must be zero, since $L_{Tp} = 0$ contradicts the definition of a patch.

[45] In this study, we calculated the Thorpe L_{Tp} scales inside the microstructure patches. The CDF of the Thorpe scale for MT patches $F(L_{Tp})$ shown in Figure 10b can be fitted by lognormal distribution in the range 0.05 m < L_{Tp} < ~0.4 m, which covers ~85% of the data. The parameters of the distribution are $\mu = -2.46 \pm 0.05$ and $\sigma_{L_{Tp}} = 0.52 \pm 0.04$. The mean value $\langle L_{Tp} \rangle = 0.10$ m and the median value $med(L_{Tp}) = 0.08$ m. The K-S test for lognormal models, however, is very close to its critical value at a level of 95%, and the goodness of the fit for L_{Tp} is lower than that for h_p.

4.3.3. The Normalized Patch Thorpe Scale L_{Tp}/h_p

[46] The CDF of the normalized patch Thorpe scale L_{Tp}/h_p is plotted in Figure 10c for the patches detected in the MT. Therefore, we explored several statistical models that may be represented as the probability distribution of L_{Tp}/h_p. One such model is the *Weibull* [1951] distribution, which was suggested by *Lozovatsky and Erofeev* [1993] as a way of approximating the CDFs of the fine structure inhomogeneities of N^2 on the assumption that stratification has the highest probability of being destroyed by turbulence in the layers of random thickness with the lowest N^2. Using the analogy between breaking events and turbulent overturns responsible for random generation of quasi-homogeneous (mixed) fine structure layers and the generation of turbulent patches, we can apply this approach to the distribution of L_{Tp}/h_p.

[47] The Weibull distribution

$$F\left(\frac{L_{Tp}}{h_p}\right) = 1 - \exp\left[-\left(\frac{1}{\lambda_w}\left(\frac{L_{Tp}}{h_p}\right)\right)^{c_w}\right] 0 < \frac{L_{Tp}}{h_p} < \infty \quad (8)$$

is specified by the scale λ_w and shape c_w parameters, which are related to the mean $\langle L_{Tp}/h_p \rangle$ and root mean square (rms) σ_{L_{Tp}/h_p} values of L_{Tp}/h_p through the Gamma function $\Gamma(x) = \int_0^\infty t^{x-1} e^{-t} dt$ as follows,

$$\langle L_{Tp}/h_p \rangle = \lambda_w \Gamma(\Phi), \text{ where } \Phi \equiv 1 + \frac{1}{c_w} \quad (9a)$$

and

$$\sigma_{L_T}/h_p = \lambda_w^2 \left[\Gamma(\Theta) - \Gamma^2(\Phi)\right], \text{ where } \Theta \equiv 1 + \frac{2}{c_w}. \quad (9b)$$

[48] It should be noted that the Gamma function in equations (9a) and (9b) depends only on the shape parameter c_w.

[49] The Weibull model fits the empirical $F(L_{Tp}/h_p)$ well in the range $0.07 < L_{Tp}/h_p < 0.5$, which covers ~95% of the distribution, leaving out only 5% of the smallest L_{Tp}/h_p (Figure 10c, solid line). The maximum likelihood estimates of the scale and shape parameters with 95% confidence intervals are $\lambda_w = 0.21 \pm 0.02$ and $c_w = 1.94 \pm 0.16$. It is evident that Weibull distribution is a good estimator of the normalized patch Thorpe scale in the metalimnion.

[50] The Weibull model has also been applied to the distribution of the Thorpe scale in a weakly stratified surface layer of the Boadella reservoir (Catalonia, Spain) during a period of wind-induced turbulence [*Roget et al.*, 2006]. Because the entire surface layer was turbulent during the period of measurements, its depth could be considered as h_p and it is therefore possible to compare the distributions of L_{Tp}/h_p in the Boadella reservoir and Lake Banyoles. Although the scale parameters of the corresponding Weibull approximations for Boadella and Banyoles are very different, the shape parameters c_w appear to be almost the same. In Boadella, $c_w = 2.0$ with a 95% confidence interval between 1.74 and 2.30; in Banyoles, $c_w = 1.94 \pm 0.16$. This might be a coincidence, but it is also possible that the value $c_w \sim 2$ of the shape parameter is related to the nature of turbulence, which associated with shear instability in both cases. When L_T was analyzed in two double-diffusion convective layers with constant but different thicknesses h_p [*Sanchez and Roget*, 2007], it was found that the distributions of L_{Tp}/h_p could be approximated with a 95% of confidence by the Weibull model with $c_w = 4.2$ for the both layers. This may indicate that the shape parameter of the Weibull distribution of the normalized patch Thorpe scale can characterize different mechanisms in the origin of the microstructure.

[51] Since the patch Thorpe scale cannot exceed the size of a patch (specifically for turbulent events related to individual overturns) the probability distribution of L_{Tp}/h_p has to be defined on a finite domain $[a, b]$, where $a = 0$ and b are its lower and upper boundaries. One of the continuous distributions that satisfies this condition is beta distribution [*Mood et al.*, 1974] (see review by *Evans et al.* [2000]) with the probability distribution function (pdf)

$$pdf_B(x) = \frac{x^{m-1}[b-x]^{q-1}}{B(m,q)b^{m+q-1}}, 0 < x < b, \quad (10)$$

where m and q are positive parameters of the beta function $B(m, q) = \int_0^1 t^{m-1}(1-t)^{q-1}dt$.

[52] The beta distribution fit shown in Figure 10c coincides with the Weibull CDF for the upper 95% of the entire data set. Parameters of the model are $m = 2.56 \pm 0.47$ and $q = 10.65 \pm 2.07$ ($b = 1$), and the mean value $\langle L_{Tp}/h_p \rangle = 0.19$.

[53] The Weibull and beta approximations were tested using Kolmogorov-Smirnov statistics with a 95% confi-
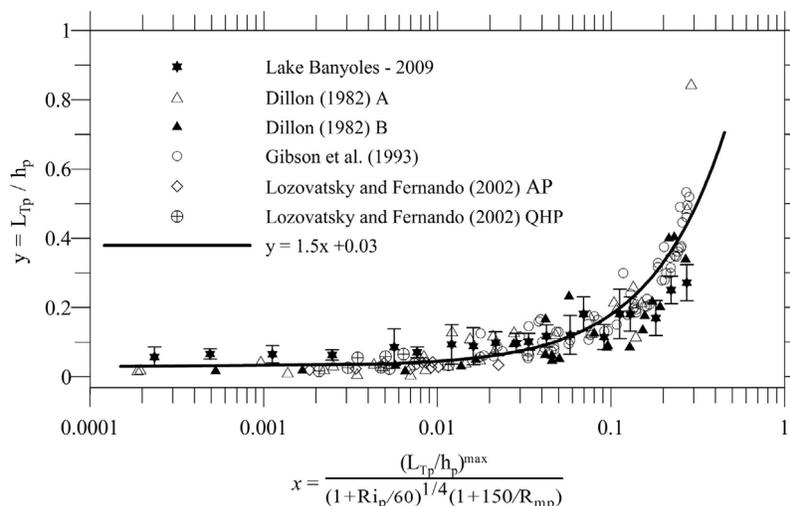
Figure 11. The normalized patch Thorpe scale L_{Tp}/h_p as a function of the patch Richardson Ri_p and mixing Reynolds R_{mp} numbers (see text for details).

dence level. In the case of the Weibull distribution, the p-value, the K-S statistics and its critical value are 0.21, 0.060, and 0.076 respectively, while for the beta model they are 0.35, 0.052, and 0.076. In both cases, K-S statistics are less than the critical value, so neither distribution can be rejected as a probability model for the empirical CDF at the 95% confidence level. The p-value shows that the probability is higher for the beta model than for the Weibull distribution. If we run the test for the 80% confidence level then the Weibull model should be rejected, but not the beta one. It should be noted that the upper limit of the random variable for the beta model is 1, although $\max(L_{Tp}/h_p) < 1$.

4.3.4. Parameterization of the Normalized Thorpe Scale

[54] The Thorpe scale, L_T, can serve as a good estimator of a characteristic turbulent scale that is used in semi-empirical closures of turbulent mixing in stratified flows. If L_T can be related to the patch size h_p, then the analysis of patch turbulence can be simplified by employing the algorithm of patch identification in a particular layer. It was shown in Section 4.2 that the ratio L_{Tp}/h_p varied in the SL depending on the state of turbulence, which is related to the age of the patch [*Smyth and Moum*, 2000; *Smyth et al.*, 2001]. The median value of L_{Tp}/h_p in the MT of Lake Banyoles was 0.18, which is more than twice the $med(L_{Tp}/h_p) = 0.07$ reported by *Moum* [1996] for large ocean patches detected in the upper part of the main thermocline. It seems the microstructure patches in the lake were mainly observed at an earlier stage of their evolution than was the case with the ocean patches. In general, the value of L_{Tp}/h_p is determined by a number of external and internal parameters, which include time at the initial stages of L_{Tp}/h_p evolution, but which could be governed by a balance between buoyancy and inertial forces, if turbulence in a patch is sustained by, let us say, ambient shear. For such environments, *Lozovatsky and Fernando* [2002] introduced a parameterization of L_{Tp}/h_p taking into account its dependence on the so-called patch Richardson number, $Ri_p = N^2 h_p^4/K_T^2$, and the patch mixing Reynolds number, $R_{mp} = K_T/\nu$, where the buoyancy frequency of the background stratification is N^2,

diffusivity is K_T, and molecular viscosity is ν. For geophysical flows (specifically, the Black Sea coastal zone) it was found that

$$\frac{L_{Tp}}{h_p} = 1.5\,x + 0.03; \quad x = \frac{\left(L_{Tp}/h_p\right)^{\text{max}}}{\left(1 + Ri_p/Ri_{pc}\right)^{1/4}\left(1 + R_{mpc}/R_{mp}\right)},$$
(11)

where x is the non-dimensional argument, $(L_{Tp}/h_p)^{\text{max}}$ is an asymptotic constant that was estimated to be equal to 0.3, and Ri_{pc} and R_{mpc} are characteristic values of Ri_p and R_{mp} equal to 60 and 150 respectively.

[55] We tested equation (11) for MT turbulent patches in Lake Banyoles, considering only patches of $h_p > 25$ cm. The total number of these patches was 281. For about 90% of the patches, the buoyancy Reynolds number exceeded 30, signifying active turbulence. The bin-averaged values of L_{Tp}/h_p are shown in Figure 11 and compared with equation (11) using $(L_{Tp}/h_p)^{\text{max}} = 0.45$ rather than the original 0.3 of *Lozovatsky and Fernando* [2002]. Although the Banyoles samples sit slightly above the line specified by equation (11) for low values of the argument x, they are consistent with previous observations of patch turbulence in the ocean [*Dillon*, 1982; *Gibson et al.*, 1993], and marine coastal waters [*Lozovatsky and Fernando*, 2002]. It should noted that the modified value of $(L_{Tp}/h_p)^{\text{max}} = 0.45$ in equation (11) is close to $(L_{Tp}/h_p)^{\text{max}} = 1/\sqrt{3} = 0.57$, which is the case for a single Z-shaped inviscid overturn without mixing [*Gibson*, 1987]. *Smyth et al.* [2001] also indicated that $(L_{Tp}/h_p)^{\text{max}}$ is close to 0.5 for a young overturn. Based on geometry, *Gibson* [1987] also proposed a slotted Z-model for an isolated turbulent mixing event where $L_{Tp}/h_p = 0.41$, but *De Silva and Fernando* [1992] argued that this model is valid only for the initial stages of mixing. Their laboratory experiments with sustained grid turbulence showed that L_{Tp}/h_p increases with time during the growing phase of a turbulent patch, which is consistent with the direct numerical simulations (DNS) of *Smyth et al.* [2001], but in this case $(L_{Tp}/h_p)^{\text{max}}$ tends to a constant value ~0.27. A similar result, $(L_{Tp}/h_p)^{\text{max}} \sim 0.29$, was obtained by *De Silva et al.* [1996]
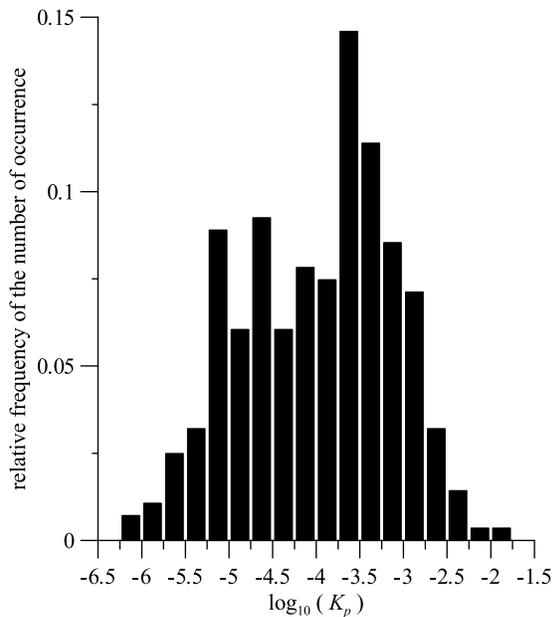
Figure 12. The histogram of the logarithm of turbulent diffusivities in microstructure patches for the entire data set of 281 patches.

when they were studying the cores of collapsed billows in a series of laboratory experiments. The asymptotic value of $(L_{Tp}/h_p)^{max}$ may depend slightly on the turbulence generation mechanism, but it is safe to suggest that it is confined to between 0.25 and 0.5. For our data, the best estimate of $(L_{Tp}/h_p)^{max}$ is 0.45. General dependence of the normalized Thorpe scale on the parameters of background stratification and patch turbulence, which is given by equation (11), agrees well with microstructure measurements in deep and coastal oceans and is now also supported by the data obtained in a small lake.

4.3.5. Intermittent Mixing and Buoyancy Fluxes

[56] Small-scale microstructure measurements make it possible to estimate the vertical diffusivities $K_p = \gamma \ \varepsilon/N^2$ [Osborn, 1980] in stratified lakes [Ravens et al., 2000; Etemad-Shahidi and Imberger, 2006; Roget et al., 2006], using the dissipation rate ε and the buoyancy frequency N, which are calculated for individual patches (larger than 25 cm) rather than at equally segmented individual profiles [Lozovatsky and Fernando, 2002; Fer et al., 2004; Liu et al., 2009]. The mixing efficiency $\gamma = 0.2$ for active turbulence [Oakey, 1982], but in a wide range of Ri and Re it is a function of these governing parameters [e.g., Ivey et al., 2008]

[57] To characterize vertical mixing across the entire thermocline using K_p, an appropriate averaging procedure needs to be utilized. We calculated the averaged diffusivity $\overline{K}_{MT}^i$ for every i profile taking into account that intermittent mixing episodes occupied only a specific fraction of the thickness of the MT. By averaging a large number of turbulent patches over a specified domain (the MT in our case) during relatively long-standing stable background conditions [Nash and Moum, 2002] a representative estimate of $\overline{K}_{MT}$ can be deduced. In our case a number of daily measured

profiles were obtained under light breezy winds. Hence, the profile averaged diffusivity is calculated as follows:

$$\overline{K}_{MT}^i = \left(\sum_j h_p^j K_p^j + \left(\overline{H}_{MT}^i - \overline{H}_p^i \right) \times D_T \right) \Big/ \overline{H}_p^i, \qquad (12)$$

where the superscript i represents the number of the profile, $\overline{H}_p^i$ is the fraction of the MT occupied by turbulent patches, $\overline{H}_{MT}^i$ is the mean thickness of the MT, h_p^j and K_p^j are the thickness and diffusivity of the individual patch j, and $D_T = 1.4 \times 10^{-7}$ m^2 s^{-1} is the molecular diffusivity.

[58] Only patches with $h_p^j > 25$ cm were used in line with the limitations of the ε calculation. It should be noted that large patches mostly contribute to the total mixing rate in pycnoclines [Gregg et al., 1986; Yamazaki and Lueck, 1987]. The total number of MT patches with $h_p > 25$ cm was 281, which is ~90% of the total number of detected patches.

[59] The state of turbulence in the patches was also evaluated using the buoyancy Reynolds number Re_b. It was found that for 90% of the patches $Re_b > 30$, which indicate active turbulence (see Section 3.2.2.). The mean Re_b for all patches was 2400, and the median 645.

[60] By averaging $\overline{K}_{MT}^i$ over the chosen number of profiles $i = 2, 3, \ldots 281$, a characteristic $\overline{K}_{MT}$ can be obtained for a specific time period. It is important to note that $\overline{K}_{MT}$ represents the mean vertical diffusivity across the MT only for relatively stable background conditions (light afternoon winds) observed in mid-summer during the period of field measurements. The histogram of the distribution of $\log_{10}(K_p.)$ for all turbulent patches is shown in Figure 12. The diffusivities ranged between 7.6×10^{-7} and 1.4×10^{-2} m^2 s^{-1} with a median value of 1.29×10^{-4} m^2 s^{-1}. The distribution is slightly skewed toward high values, with the skewness S equalling -0.20. For approximately symmetric distributions (where the skewness is between -0.5 and 0.5 [Bulmer, 1979]) the mean value of K_p can be estimated as the geometric mean $\hat{K}_p$ [Borradaile, 2003]. We calculated this value using the bootstrap method [Efron and Tibshirani, 1993]. The bootstrap samples used for the averaging were ten times the actual number of samples. The campaign averaged $\hat{K}_p = 1.03 \times 10^{-4}$ m^2 s^{-1} with 95% bootstrapped confidence limits of 8.50×10^{-5} m^2 s^{-1} and 1.22×10^{-4} m^2 s^{-1}.

[61] The estimate of effective mean diffusivity in the thermocline $\overline{K}_{MT}^i$ computed using equation (12) for the entire period of observations ($i = 281$ profiles) was $\overline{K}_{MT} = 7.03 \times 10^{-5}$ m^2 s^{-1}, which corresponds well to the averaged vertical diffusivities in stratified interiors of lakes and oceans [Ledwell and Watson, 1991; Alford and Pinkel, 2000; Sharples et al., 2001; Etemad-Shahidi and Imberger, 2006]. Values ranging between 10^{-4}–10^{-5} m^2 s^{-1} were reported by Roget et al. [2006] for measurements on a shallow stratified shelf. The estimate of $\overline{K}_{MT}$ obtained, however, may be subject to relatively high variability considering the rather short period of our observations and temporal variations in the internal seiche characteristics in the lake.

[62] In order to characterize vertical transport across the MT we first computed the buoyancy flux for each detected patch as $J_{bp} = K_p N_p^2$ and then averaged it over the entire data set in the same way as was done for K_p (equation (12)) to provide the buoyancy flux for non-turbulent segments
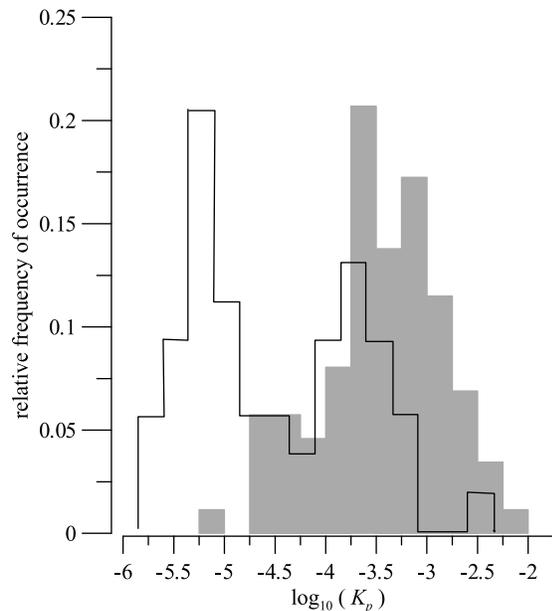
Figure 13. The histogram of the logarithm of turbulent diffusivities in microstructure patches for July 1 (gray bars) and June 25 (open bars).

$J_{bnt} = D_T N_{nt}^2$. The probability distribution of $\log_{10}(J_{bp})$ can be considered approximately normal, with the skewness S equaling -0.38. The geometrically averaged $\hat{J}_{bp}$ was $(2.29 \pm 0.46) \times 10^{-7}$ W kg^{-1}. The effective mean buoyancy flux $\overline{J}_{MT}$ across the main thermocline computed similarly to $\overline{K}_{MT}^i$ (equation (12)) and when averaged for the entire period of observations ($i = 281$) was found to be 1.90×10^{-7} W kg^{-1}.

[63] We analyzed the role of internal seiches as the major source of vertical mixing in the thermocline, comparing the distributions of K_p for June 25 and July 1, when the measurement site was affected by internal seiches in different phases (see Section 4.1). The histograms of two distributions of $\log_{10}(K_p)$ are shown in Figure 13. It should be noted that for July 1 the histogram is relatively symmetric, but not for June 25. About 60% of the data show $\log_{10}(K_p) < -4$, despite of several large diffusivity values in the record. The number of turbulent patches detected on June 25 (55) was significantly less than on July 1 (87). Temporal variations in the thermocline displacement were small (only of a few centimeters) on June 25, but on July 1 they were large (maximum values of about ~0.5 m), as can be seen in Figures 3 and 5. Note that large temporal variations in the vertical displacements correspond to a seiche phase with small vertical displacements and, as such, high horizontal velocities and maximum vertical shear. The seiche dynamics were similar on June 27. The mean patch diffusivities for June 25 and July 1 were estimated as $(4.58 \pm 1.71) \times 10^{-5}$ and $(3.65 \pm 0.80) \times 10^{-4}$ m^2 s^{-1} respectively, with the diffusivities differing by an order of magnitude depending on the phase of the internal seiche. The values obtained on June 25 are close to those reported by *Etemad-Shahidi and Imberger* [2006] in Lake Biwa and Lake Kinneret.

[64] The mean diffusivities for June 25 and July 1 were computed using only turbulent fractions, which on July 1 occupied about 19% of the MT compared to 10% on June 25.

The mean diffusivities across the MT were 1.61×10^{-4} m^2 s^{-1} and 5.73×10^{-5} m^2 s^{-1} respectively. Similar values were obtained for June 23 and June 27 (where the vertical displacements were also small) with mean diffusivities of 5.57×10^{-5} m^2 s^{-1} and 8.1×10^{-5} m^2 s^{-1} respectively.

[65] The effective buoyancy flux across the MT was $\sim1.72 \times 10^{-7}$ W kg^{-1} on June 25, which is approximately half its estimate (4×10^{-7} W kg^{-1}) for July 1. The difference is attributable to the variation in vertical shear in the MT, which is controlled by different phases of the internal seiche. The same conclusions can be drawn from June 23 and June 27 (1.39×10^{-7} W kg^{-1} and 2.11×10^{-7} W kg^{-1}).

5. Summary

[66] Microstructure patchiness in stable stratified layers was studied using multiple profiling measurements in Lake Banyoles (Catalonia, Spain) under weak and moderate winds. The probability distributions of patch sizes h_p and turbulent scales (the patch Thorpe L_{Tp} scale and the normalized patch Thorpe L_{Tp}/h_p scale) were analyzed. Microstructure patches were detected across the entire water column but we focused our analysis on the main thermocline in the interior of the lake.

[67] Free-falling profiler measurements and a comprehensive algorithm of the data processing allowed us to identify small turbulent patches, calculate the patch Thorpe scales and analyze the corresponding probability distributions of h_p, L_{Tp}, and the normalized patch Thorpe scale L_{Tp}/h_p. It should be noted that the lack of small patches in the CTD-based data [e.g., *Peters et al.*, 1995; *Stansfield et al.*, 2001; *Lee et al.*, 2009] negatively influences basic patch statistics and their probability distribution.

[68] Table 2 summarizes parameters of the probability distributions of h_p, L_{Tp}, and L_{Tp}/h_p separately for the entire set of patches (very small patches of $L_{Tp} < 4$ cm were not considered due to noise restrictions) and for patches of $h_p > 25$ cm, which were used for the calculation of ε. The goodness of the fits and the appropriate range of the corresponding variables for the proposed CDFs are shown in Table 2.

[69] For the entire data set, the empirical CDF of patch sizes can be well fitted by a lognormal model deviating from lognormality by only CDF(h_p) < 0.03 and CDF(h_p) > 0.97. When small patches ($h_p < 25$ cm) are not included in the analysis of the CDF, the lower tail starts to deviate from the lognormal distribution at a much higher CDF(h_p) ≈ 0.15 (see Table 2). The lack of vertical resolution, which prevents identification of small patches, may explain sharp cuts in the tails of the lognormal model reported by several authors [*Lozovatsky et al.*, 1993; *Stansfield et al.*, 2001].

[70] A sharp cut in the lower tail of the L_{Tp} distribution is also observed for 15% of our data, which could be a result of the constraints of the patch identification method ($L_{Tp} > 4$ cm). When only patches with $h_p > 25$ cm were analyzed, the range of validity for the lognormal fit to the empirical CDF(L_{Tp}) extended from an initial 15% to 8%. Insufficient resolution of profiling measurements may explain sharp tails at small scales of L_T probability plots [*Alford and Pinkel*, 2000; *Stansfield et al.*, 2001] and the difficulties with fitting data to lognormal distribution reported by *Kitade et al.* [2003] and L. M. Huzzey and T. M.

Table 2. Statistical Parameters of Lognormal Distributions of h_p and L_{Tp} and the Weibull and Beta Distributions of L_{Tp}/h_p in Patches From the Main Thermocline

Parameters CDF	Lognormal Distribution				K-S Goodness-of-Fit Test		
	μ	σ	$med(h_p)$ (m)	$\langle h_p \rangle$ (m)	p-Value	K-S Statistics[a]	Range Validity (m)
Entire data set ($L_{Tp} > 4$ cm)	−0.65	0.75	0.50	0.69	0.89	0.032 < 0.076	0.14 < h_p < 2.15 (3–97% of data)
Patches with $h_p > 25$ cm	−0.42	0.60	0.62	0.78	0.19	0.066 < 0.083	0.35 < h_p < 2.00 (15–95% of data)

Parameters CDF	Lognormal Distribution				K-S Goodness-of-Fit Test		
	μ	σ	$med(L_{Tp})$ (m)	$<L_{Tp}>$ (m)	p-Value	K-S Statistics[a]	Range of Validity (m)
Entire data set ($L_{Tp} > 4$ cm)	−2.46	0.52	0.08	0.10	0.053	0.074 < 0.076	0.05 < L_{Tp} < 0.40 (15–99% of data)
Patches with $h_p > 25$ cm	−2.39	0.51	0.09	0.11	0.51	0.051 < 0.083	0.044 < L_{Tp} < 0.36 (8–99% of data)

Parameters CDF	Weibull Distribution		K-S Goodness-of-Fit Test		
	λ_w	c_w	p-Value	K-S Statistics[a]	Range of Validity
Entire data set ($L_{Tp} > 4$ cm)	0.21	1.94	0.21	0.060 < 0.076	0.07 < L_{Tp}/h_p < 0.5 (5–99% of data)
Patches with $h_p > 25$ cm	0.19	1.99	0.21	0.065 < 0.083	0.05 < L_{Tp}/h_p < 0.4 (8–97% of data)

Parameters CDF	Beta Distribution			K-S Goodness-of-Fit Test		
	m	q	b	p-Value	K-S Statistics[a]	Range of Validity
Entire data set ($L_{Tp} > 4$ cm)	2.56	10.65	1	0.35	0.052 < 0.076	0.05 < L_{Tp}/h_p < 0.5 (<5–99% of data)
Patches with $h_p > 25$ cm	2.80	13.81	1	0.38	0.056 < 0.083	0.04 < L_{Tp}/h_p < 0.4 (<5–97% of data)

[a]K-S statistics value is compared to the critical value of the test.

Powell (Tidal variation in turbulent eddy sizes in an estuary, unpublished manuscript, 2005). It is worth noting, however, that small patches do not substantially modify the parameters of L_{Tp} distribution, because large eddies dominate the Thorpe scale values [*Stansfield et al.*, 2001; *Lorke and Wüest*, 2002].

[71] It has been suggested [*Lozovatsky and Fernando*, 2002] that the ratio L_{Tp}/h_p depends on the patch Richardson number $Ri_p = N^2 h_p^4 / K_p^2$ and the patch mixing Reynolds number $R_{mp} = K_p/\nu$ and can be parameterized by equation (11). The patch Richardson number reflects the balance between buoyancy and small scale shear inside patches. This shear is an integral of the dissipation spectrum between the lowest wave number proportional to $2\pi/h_p$ and the highest possible wave number specified by the shear signal. The diffusivity K_p is a measure of this shear and the powers of N, K_p and h_p follow the requirement to make the combination non-dimensional. The ratio L_{Tp}/h_p decreases with Ri_p, because the patch Richardson number is an analog of the inverse Ozmidov scale $L_N^{-1} \sim (N^3/\varepsilon)^{1/2}$.

[72] The empirical CDF of L_{Tp}/h_p is well approximated by Weibull and beta distributions in a range covering about 95% of the data. The median value of L_{Tp}/h_p (0.17) appears to be about two times larger than that reported by *Moum* [1996] for a series of ocean patches detected in the main pycnocline of the North Atlantic [$med(L_{Tp}/h_p) = 0.07$]. The size of the oceanic patches ranged between 3 and 15 m, while the lake patches were much smaller (the largest being $h_p < 4$ m). The background stratification in the ocean (a characteristic $N \sim 0.005$ s^{-1}) was much weaker than in the lake. Ocean patches selected for the analysis were large and not very energetic (with ε less than 10^{-8} W kg^{-1} in more than 50% of cases). Therefore, the median of the ratio of L_{Tp}/h_p was small, suggesting that those patches were probably observed at a later stage of their evolution compared to the patches in the lake.

[73] Different phases of the oscillation cycle of internal seiches in the lake affected the vertical shear in the thermocline and, as the result, the generation of turbulent patches. The temporal variability of vertical mixing was analyzed based on the averaged vertical diffusivities estimated from the microstructure patches. When large vertical displacements of the isotherms (i.e., maximum vertical shear) were observed (July 1) the averaged diffusivity was higher than in the phase of very low internal seiche amplitude (June 25). The short period of observation may, however, have affected the robustness of the estimates of averaged diffusivities and buoyancy fluxes obtained across the thermocline.

[74] Episodic wind gusts lasting a few minutes with U_{10} exceeding 6 m s^{-1} transferred ~1.6% of the wind energy to the surface mixed layer and ~0.7% to the stratified water interior, generating large (with h_p sometimes reaching several meters) but rare microstructure patches in the hypolimnion. It is likely that sharp wind gusting generates strong horizontal fluctuations of pressure that induce short-lived strong horizontal and vertical shear instabilities that stir and mix the water interior.

[75] These large but rare turbulent events (we observed only ten of them) belong to a different statistical population from regular MT patches. Large and regular patches are supposed to be governed by different statistical regularities and correspond to different probability distribution functions. Having a long series of wind induced large patches would make it possible to obtain valuable statistical characteristics of these rare events by analyzing their CDF and comparing it with the extreme value distribution model. Special long-term field measurements are needed to shed light on this problem.

References

Alford, M. H., and R. Pinkel (2000), Observations of overturning in the thermocline: The context of ocean mixing, *J. Phys. Oceanogr.*, 30, 805–832, doi:10.1175/1520-0485(2000)030<0805:OOOITT>2.0.CO;2.

Ayyub, B. M., and M. H. McCuen (1996), *Numerical Methods for Engineers*, Prentice Hall, Upper Saddle River, N. J.

Baines, P. G. (2001), Mixing in flows down gentle slopes into stratified environments, *J. Fluid Mech.*, 443, 237–270, doi:10.1017/S0022112001005250.

Borradaile, G. (2003), *Statistics of Earth Science Data*, Springer, Berlin.

Brandl, H., K. W. Hanselmann, R. Bachofen, and J. Piccard (1993), Small-scale patchiness in the chemistry and microbiology of sediments in Lake Geneva, Switzerland, *Microbiology*, 139, 2271–2275, doi:10.1099/00221287-139-9-2271.

Bryson, R. A., and R. A. Ragotzkie (1960), On internal waves in lakes, *Limnol. Oceanogr.*, 5, 397–408, doi:10.4319/lo.1960.5.4.0397.

Bulmer, M. G. (1979), *Principles of Statistics*, Dover, Mineola, N. Y.

Casamitjana, X., and E. Roget (1993), Resuspension of sediments by focused groundwater, *Limnol. Oceanogr.*, 38, 643–656, doi:10.4319/lo.1993.38.3.0643.

Casamitjana, X., J. Colomer, E. Roget, and T. Serra (2006), Physical limnology in Lake Banyoles, *Limnetica*, 25, 181–188.

Chen-Tung, A. C., and F. J. Millero (1986), Precise thermodynamics properties for natural waters covering only the limnological range, *Limnol. Oceanogr.*, 31, 657–662, doi:10.4319/lo.1986.31.3.0657.

Crawford, W. R. (1986), A comparison of length scales and decay times of turbulence in stratified flows, *J. Phys. Oceanogr.*, 16, 1847–1854, doi:10.1175/1520-0485(1986)016<1847:ACOLSA>2.0.CO;2.

Crow, E., and K. Shimizu (1988), *Lognormal Distributions: Theory and Applications*, Marcel Dekker, New York.

D'Asaro, E. A., and G. T. Dairiki (1997), Turbulence intensity measurements in a wind-driven mixed layer, *J. Phys. Oceanogr.*, 27, 2009–2022, doi:10.1175/1520-0485(1997)027<2009:TIMIAW>2.0.CO;2.

Davis, C. S., G. R. Flierl, P. H. Wiebe, and P. J. S. Franks (1991), Micropatchiness, turbulence and recruitment in plankton, *J. Mar. Res.*, 49, 109–151, doi:10.1357/002224091784968602.

Delaney, M. P. (2003), Effects of temperature and turbulence on the predator-prey interactions between a heterotrophic flagellate and a marine bacterium, *Microb. Ecol.*, 45, 218–225, doi:10.1007/s00248-002-1058-4.

De Silva, I. P. D., and H. J. S. Fernando (1992), Some aspects of mixing in a stratified turbulent patch, *J. Fluid Mech.*, 240, 601–625, doi:10.1017/S0022112092000223.

De Silva, I. P. D., H. J. S. Fernando, F. Eaton, and D. Hebert (1996), Evolution of Kelvin-Helmholtz billows in nature and laboratory, *Earth Planet. Sci. Lett.*, 143, 217–231, doi:10.1016/0012-821X(96)00129-X.

Dillon, T. M. (1982), Vertical overturns: A comparison of Thorpe and Ozmidov length scales, *J. Geophys. Res.*, 87, 9601–9613, doi:10.1029/JC087iC12p09601.

Efron, B., and R. Tibshirani (1993), *An Introduction to the Bootstrap*, *Monogr. Stat. Appl. Probab.*, vol. 57, Chapman & Hall, New York.

Etemad-Shahidi, A., and J. Imberger (2006), Diapycnal mixing in the thermocline of lakes: Estimations by different methods, *Environ. Fluid Mech.*, 6, 227–240, doi:10.1007/s10652-005-4480-6.

Evans, M., N. Hastings, and B. Peacock (2000), Beta distribution, in *Statistical Distributions*, edited by A. C. Noel et al., pp. 34–42, Wiley, New York.

Evans, C., B. Reynolds, C. Hinton, S. Hughes, D. Norris, G. Grant, and B. Williams (2008), Effects of decreasing acid deposition and climate change on acid extremes in an upland stream, *Hydrol. Earth Syst. Sci.*, 12, 337–351, doi:10.5194/hess-12-337-2008.

Fer, I., R. Skogseth, and P. M. Haugan (2004), Mixing of the Storfjorden overflow (Swalbard Archipelago) inferred from density overturns, *J. Geophys. Res.*, 109, C01005, doi:10.1029/2003JC001968.

Ferron, B., H. Mercier, K. Speer, A. Gargett, and K. Polzin (1998), Mixing in the Romanche Fracture Zone, *J. Phys. Oceanogr.*, 28, 1929–1945, doi:10.1175/1520-0485(1998)028<1929:MITRFZ>2.0.CO;2.

Fofonoff, N. P., and R. C. Millard Jr. (1983), Algorithms for computation of fundamental properties of seawater, *Tech. Pap. Mar. Sci. 44*, U. N. Educ. Sci. and Cultural Organ., Paris.

Folkard, A. M., A. J. Sherborne, and M. J. Coates (2007), Turbulence and stratification in Priest Pot, a productive pond in a sheltered environment, *Limnology*, 8(2), 113–120, doi:10.1007/s10201-007-0207-3.

Fozdar, F., J. Parker, and J. Imberger (1985), Matching temperature and conductivity sensor response characteristics, *J. Phys. Oceanogr.*, 15, 1557–1569, doi:10.1175/1520-0485(1985)015<1557:MTACSR>2.0.CO;2.

Galbraith, P. S., and D. E. Kelley (1996), Identifying overturns in CTD profiles, *J. Atmos. Oceanic Technol.*, 13, 688–702, doi:10.1175/1520-0426(1996)013<0688:IOICP>2.0.CO;2.

Gale, E., C. Pattiaratchi, and R. Ranasinghe (2006), Vertical mixing processes in intermittently closed and open lakes and lagoons, and the dissolved oxygen response, *Estuarine Coastal Shelf Sci.*, 69, 205–216, doi:10.1016/j.ecss.2006.04.013.

Garcia-Gil, L. J., C. Borrego, L. Hugas, X. Casamitjana, and C. A. Abella (1988), Horizontal distribution of phototrophic bacterial population in an irregularly shaped meromictic basin of Banyoles Lake (Banyoles, Spain), *Sci. Gerundensis*, 14, 71–79.

Gargett, A. E., T. R. Osborn, and P. W. Nasmyth (1984), Local isotropy and the decay of turbulence in a stratified fluid, *J. Fluid Mech.*, 144, 231–280, doi:10.1017/S0022112084001592.

Gibson, C. H. (1980), Fossil temperature, salinity, and vorticity turbulence, in *Marine Turbulence*, *Elsevier Oceanogr. Ser.*, vol. 28, edited by J. J. C. Nihoul, pp. 221–257, Elsevier, Amsterdam.

Gibson, C. H. (1987), Fossil turbulence and intermittency in sampling oceanic mixing processes, *J. Geophys. Res.*, 92, 5383–5404, doi:10.1029/JC092iC05p05383.

Gibson, C. H. (1991a), Laboratory, numerical, and oceanic fossil turbulence in rotating and stratified fluid, *J. Geophys. Res.*, 96, 12,549–12,566, doi:10.1029/91JC00186.

Gibson, C. H. (1991b), Turbulence, mixing and heat flux in the ocean main thermocline, *J. Geophys. Res.*, 96, 20,403–20,420, doi:10.1029/91JC02122.

Gibson, C. H., V. N. Nabatov, and R. V. Ozmidov (1993), Measurements of turbulence and fossil turbulence near Ampere Seamount, *Dyn. Atmos. Oceans*, 19, 175–204, doi:10.1016/0377-0265(93)90036-7.

Gregg, M. C. (1980), Microstructure patches in the thermocline, *J. Phys. Oceanogr.*, 10, 915–943, doi:10.1175/1520-0485(1980)010<0915:MPITT>2.0.CO;2.

Gregg, M. C., E. A. D'Asaro, T. J. Shay, and N. Larson (1986), Observations of persistent mixing and near-inertial internal waves, *J. Phys. Oceanogr.*, 16, 856–885, doi:10.1175/1520-0485(1986)016<0856:OOPMAN>2.0.CO;2.

Hood, M., M. Fukasawa, N. Gruber, G. C. Johnson, A. Körtzinger, C. Sabine, B. Sloyan, K. Stansfield, and T. Tanhua (2010), Ship-based repeat hydrography: A strategy for a sustained global program, in *Proceedings of OceanObs'09: Sustained Ocean Observations and Information for Society*, vol. 2, edited by J. Hall et al., Eur. Space Agency, Venice, Italy, doi:10.5270/OceanObs09.cwp.44.

Imberger, J. (1985), The diurnal mixed layer, *Limnol. Oceanogr.*, 30, 737–770, doi:10.4319/lo.1985.30.4.0737.

Imberger, J. (1994), Transport processes in lakes: A review, in *Limnology Now: A Paradigm of Planetary Problems*, edited by R. Margalef, pp. 99–191, Elselvier Sci, New York.

Imberger, J. (1998), Flux paths in a stratified lake: A review, in *Physical Processes in Lakes and Oceans*, *Coastal Estuarine Stud. Ser.*, vol. 54, edited by J. Imberger, pp. 1–18, AGU, Washington, D. C.

Imberger, J., and J. C. Patterson (1990), Physical limnology, in *Advances in Applied Mechanics*, edited by T. Wu, pp. 303–475, Academic, Boston.

Itsweire, E. C., K. N. Helland, and C. W. Van Atta (1986), The evolution of grid-generated turbulence in a stably stratified fluid, *J. Fluid Mech.*, 162, 299–338, doi:10.1017/S0022112086002069.

Itsweire, E. C., J. R. Koseff, D. A. Briggs, and J. H. Ferziger (1993), Turbulence in stratified shear flows: Implications for interpreting shear-induced mixing in the ocean, *J. Phys. Oceanogr.*, 23, 1508–1522, doi:10.1175/1520-0485(1993)023<1508:TISSFI>2.0.CO;2.

Ivey, G. N., K. B. Winters, and J. R. Koseff (2008), Density stratification, turbulence, but how much mixing?, *Annu. Rev. Fluid Mech.*, 40, 169–184, doi:10.1146/annurev.fluid.39.050905.110314.

Jago, C. F., S. E. Jones, P. Sykes, and T. Rippeth (2006), Temporal variation of suspended particulate matter and turbulence in a high energy, tide-stirred, coastal sea: Relative contributions of resuspension and disaggregation, *Cont. Shelf Res.*, 26, 2019–2028, doi:10.1016/j.csr.2006.07.009.

Johnson, H. L., and C. Garrett (2004), Effects of noise on Thorpe scales and run lengths, *J. Phys. Oceanogr.*, 34, 2359–2372, doi:10.1175/JPO2641.1.

Kiørboe, T. (1997), Small-scale turbulence, marine snow formation, and planktivorous feeding, *Sci. Mar.*, 61, 141–158.

Kitade, Y., M. Matsuyama, and J. Yoshida (2003), Distribution of overturn induced by internal tides and Thorpe scale in Uchiura Bay, *J. Oceanogr.*, 59, 845–850, doi:10.1023/B:JOCE.0000009575.29339.35.

Kocsis, O., B. Mathis, M. Gloor, M. Schurter, and A. Wüest (1998), Enhanced mixing in narrows: A case study at the Minau sill (Lake Constance), *Aquat. Sci.*, *60*, 236–252, doi:10.1007/s000270050039.

Kocsis, O., H. Prandke, A. Stips, A. Simon, and A. Wüest (1999), Comparison of dissipation of turbulent kinetic energy determined from shear and temperature microstructure, *J. Mar. Syst.*, *21*, 67–84, doi:10.1016/S0924-7963(99)00006-8.

Kolmogorov, A. N. (1941), On log-normal distribution of the sizes of particle in the course of breakdown, *Dokl. Akad. Sci.*, *31*, 99–101.

Lagadeuc, Y. (2005), Nutrient fluxes toward phytoplankton: Is it useful to consider turbulence intermittency?, *Acta Biotheor.*, *53*, 371–379, doi:10.1007/s10441-005-4891-2.

Lande, R., and M. R. Lewis (1989), Models of photoadaptation and pthotosynthesis by algal cells in a turbulent mixing layer, *Deep Sea Res. Part A*, *36*, 1161–1175, doi:10.1016/0198-0149(89)90098-8.

Larsen, R. J., and M. L. Marx (1986), *An Introduction to Mathematical Statistics and its Applications*, Prentice-Hall, Englewood Cliffs, N. J.

Lazaro, B. J., and J. C. Lasheras (1992), Particle dispersion in the developing free shear layer. Part 2. Forced flow, *J. Fluid Mech.*, *235*, 179–221, doi:10.1017/S0022112092001083.

Ledwell, J. R., and A. Bratkovich (1995), A tracer study of mixing in the Santa Cruz Basin, *J. Geophys. Res.*, *100*, 20,681–20,704, doi:10.1029/95JC02164.

Ledwell, J. R., and A. J. Watson (1991), The Santa Monica basin tracer experiment: A study of diapycnical and isopycnical mixing, *J. Geophys. Res.*, *96*, 8695–8718, doi:10.1029/91JC00102.

Lee, I. H., R. C. Lien, J. T. Liu, and W. Chuang (2009), Turbulent mixing and internal tides in Gaoping (Kaoping) submarine canyon, Taiwan, *J. Mar. Syst.*, *76*, 383–396, doi:10.1016/j.jmarsys.2007.08.005.

Lewis, M. R., E. P. W. Horne, J. J. Cullen, N. S. Oakey, and T. Platt (1984), Turbulent motions may control phytoplankton photosynthesis in the upper ocean, *Nature*, *311*, 49–50, doi:10.1038/311049a0.

Liu, Z., H. Wei, I. D. Lozovatsky, H. J. S. Fernando (2009), Late summer stratification, internal waves, and turbulence in the Yellow Sea, *J. Marine Syst.*, *77*, 459–472, doi:101016/.j.jmarsys.2008.11.001.

Lombardo, C. P., and M. C. Gregg (1989), Similarity scaling of viscous and thermal dissipation in a convecting surface boundary layer, *J. Geophys. Res.*, *94*, 6273–6284, doi:10.1029/JC094iC05p06273.

Lorke, A., and A. Wüest (2002), Probability density of displacement and overturning length scales under diverse stratification, *J. Geophys. Res.*, *107*(C12), 3214, doi:10.1029/2001JC001154.

Lorke, A., F. Peeters, and A. Wüest (2005), Shear-induced convective mixing in bottom boundary layers on slopes, *Limnol. Oceanogr.*, *50*, 1612–1619, doi:10.4319/lo.2005.50.5.1612.

Lozovatsky, I. D., and A. Y. Erofeev (1993), Statistical approach to eddy viscosity simulation for numerical models of the upper turbulent layer, *J. Mar. Syst.*, *4*, 391–399, doi:10.1016/0924-7963(93)90023-F.

Lozovatsky, I. D., and H. J. S. Fernando (2002), Mixing on a shallow shelf of the Black Sea, *J. Phys. Oceanogr.*, *32*, 945–956, doi:10.1175/1520-0485(2002)032<0945:MOASSO>2.0.CO;2.

Lozovatsky, I. D., A. S. Ksenofontov, A. Y. Erofeev, and C. H. Gibson (1993), Modeling of the evolution of vertical structure in the upper ocean by atmospheric forcing and intermittent turbulence in the pycnocline, *J. Mar. Syst.*, *4*, 263–273, doi:10.1016/0924-7963(93)90013-C.

Lozovatsky, I., E. Roget, and H. J. S. Fernando (2005), Mixing in shallow waters: Measurements, processing and applications, *J. Ocean Univ. China*, *4*, 293–305, doi:10.1007/s11802-005-0050-2.

Lueck, R. G., and J. J. Picklo (1990), Thermal inertia of conductivity cells: Observations with a Sea-Bird Cell, *J. Atmos. Oceanic Technol.*, *7*, 756–768, doi:10.1175/1520-0426(1990)007<0756:TIOCCO>2.0.CO;2.

MacIntyre, S., and R. Jellison (2001), Nutrient fluxes from upwelling and enhanced turbulence at the top of the pycnocline in Mono Lake, California, *Hydrobiologia*, *466*, 13–29, doi:10.1023/A:1014563914112.

MacIntyre, S., A. L. Alldredge, and C. C. Gotschalk (1995), Accumulation of marine snow at density discontinuities in the water column, *Limnol. Oceanogr.*, *40*, 449–468, doi:10.4319/lo.1995.40.3.0449.

MacIntyre, S., K. M. Flynn, R. Jellison, and J. R. Romero (1999), Turbulent mixing induced by nonlinear internal waves in Mono Lake, California, *Limnol. Oceanogr.*, *44*, 512–529, doi:10.4319/lo.1999.44.3.0512.

McPhee-Shaw, E. E., and E. Kunze (2002), Boundary-layer intrusions from a sloping bottom: A mechanism for generating intermediate nepheloid layers, *J. Geophys. Res.*, *107*(C6), 3050, doi:10.1029/2001JC000801.

Middleton, J. H., and T. D. Foster (1980), Fine structure measurements in a temperature-compensated halocline, *J. Geophys. Res.*, *85*, 1107–1122, doi:10.1029/JC085iC02p01107.

Mood, A. M., F. A. Graybill, and D. C. Boes (1974), *Introduction to the Theory of Statistics*, McGraw Hill, New York.

Moreno-Amich, R., and E. Garcia Berthou (1989), A new bathymetric map based on echo-sounding and morphometrical characterization of the Lake of Banyoles, *Hydrobiologia*, *185*, 83–90, doi:10.1007/BF00006070.

Moum, J. N. (1996), Energy-containing scales of turbulence in the ocean thermocline, *J. Geophys. Res.*, *101*, 14,095–14,109, doi:10.1029/96JC00507.

Moum, J. N., A. Perlin, J. M. Klymak, M. D. Levine, T. Boyd, and P. M. Kosro (2004), Convectively driven mixing in the bottom boundary layer, *J. Phys. Oceanogr.*, *34*, 2189–2202, doi:10.1175/1520-0485(2004)034<2189:CDMITB>2.0.CO;2.

Muelbert, J. H., M. R. Lewis, and D. E. Kelley (1994), The importance of small-scale turbulence in the feeding of herring larvae, *J. Plankton Res.*, *16*, 927–944, doi:10.1093/plankt/16.8.927.

Münnich, M., A. Wüest, and D. M. Imboden (1992), Observations of the second vertical mode of the internal seiche in an alpine lake, *Limnol. Oceanogr.*, *37*, 1705–1719, doi:10.4319/lo.1992.37.8.1705.

Nash, J. D., and J. N. Moum (2002), Microstructure estimates of turbulent salinity flux and the dissipation spectrum of salinity, *J. Phys. Oceanogr.*, *32*, 2312–2333, doi:10.1175/1520-0485(2002)032<2312:MEOTSF>2.0.CO;2.

Nishri, A., J. Imberger, W. Eckert, I. Ostrovsky, and Y. Geifman (2000), The physical regime and the respective biogeochemical processes in the lower water mass of Lake Kinneret, *Limnol. Oceanogr.*, *45*, 972–981, doi:10.4319/lo.2000.45.4.0972.

Oakey, N. (1982), Determination of the rate of dissipation of turbulent energy from simultaneous temperature and velocity shear microstructure measurements, *J. Phys. Oceanogr.*, *12*, 256–271, doi:10.1175/1520-0485(1982)012<0256:DOTROD>2.0.CO;2.

O'Brien, K., D. Meyer, A. Waite, G. Ivey, and D. Hamilton (2004), Disaggregation of *Microcystis aeruginosa* colonies under turbulent mixing: Laboratory experiments in a grid-stirred tank, *Hydrobiologia*, *519*, 143–152, doi:10.1023/B:HYDR.0000026501.02125.

Osborn, T. (1980), Estimates of the local rate of diffusion from dissipation measurements, *J. Phys. Oceanogr.*, *10*(1), 83–89, doi:10.1175/1520-0485(1980)010<0083:EOTLRO>2.0.CO;2.

Panchev, S., and D. Kesich (1969), Energy spectrum of isotropic turbulence at large wavenumbers, *C. R. Acad. Bulg. Sci.*, *22*, 627–630.

Perez-Losada, J., E. Roget, and X. Casamitjana (2003), Evidence of high vertical wave-number behaviour in a continuously stratified reservoir, *J. Hydrol. Eng.*, *129*, 734–737, doi:10.1061/(ASCE)0733-9429(2003)129:9(734).

Peters, F., and C. Marrasé (2000), Effects of turbulence on plankton: An overview of experimental evidence and some theoretical considerations, *Mar. Ecol. Prog. Ser.*, *205*, 291–306, doi:10.3354/meps205291.

Peters, F., L. Arin, C. Marrasé, E. Berdalet, and M. M. Sala (2006), Effects of small-scale turbulence on the growth of two diatoms of different size in a phosphorus-limited medium, *J. Mar. Syst.*, *61*, 134–148, doi:10.1016/j.jmarsys.2005.11.012.

Peters, H., M. C. Gregg, and T. B. Sanford (1995), Detail and scaling of turbulent overturns in the Pacific Equatorial Undercurrent, *J. Geophys. Res.*, *100*, 18,349–18,368, doi:10.1029/95JC01360.

Piera, J., E. Roget, and J. Catalan (2002), Turbulent patch identification in microstructure profiles: A method based on wavelet denoising and Thorpe displacement analysis, *J. Atmos. Oceanic Technol.*, *19*, 1390–1402, doi:10.1175/1520-0426(2002)019<1390:TPIIMP>2.0.CO;2.

Planella, J., X. Sanchez, and E. Roget (2009), Delving deeper into the hydrodynamics of karstic lakes: One more step to improve environmental management and ecohydrology, in *WMHE2009, Proceedings International Symposium on Water Management and Hydraulic Engineering*, edited by C. Popovska and M. Jovanovski, pp. 815–826, Ss. Cyril and Methodius Univ., Skopje.

Pozdynin, V. D. (2002), *Small-Scale Turbulence in the Ocean (in Russian)*, Nauka Publ., Moscow.

Prandke, H., and A. Stips (1998), Test measurements with an operational microstructure turbulence profiler: Detection limit of dissipations rates, *Aquat. Sci.*, *60*, 191–209.

Prandke, H., K. Holtsth, and A. Stips (2000), *MITEC Technology Development: The Microstructure-Turbulence Measuring System MSS*, Ispra Jt. Res. Cent., Eur. Comm., Ispra, Italy.

Puig, P., A. Palanques, J. Guillen, and M. El Kathab (2004), Role of internal waves in the generation of nepheloid layers on the northwestern Alboran slope: Implications for continental margin shaping, *J. Geophys. Res.*, *109*, C09011, doi:10.1029/2004JC002394.

Ravens, T. M., O. Kocsis, N. Granin, and A. Wüest (2000), Small-scale turbulence and vertical mixing in Lake Baikal, *Limnol. Oceanogr.*, *45*, 159–173, doi:10.4319/lo.2000.45.1.0159.

Rhodes, C. J., and A. M. Reynolds (2007), The influence of search strategies and homogeneous isotropic turbulence on planktonic contact rates, *Europhys. Lett.*, *80*, 60,003–60,008, doi:10.1209/0295-5075/80/60003.

Roget, E., G. Salvadé, F. Zamboni, and J. E. Llebot (1993), Internal waves in a small lake with a thick metalimnion, *Verh. Internat. Verein. Limnol.*, *25*, 91–99.

Roget, E., G. Salvadé, and F. Zamboni (1997), Internal seiche climatology in a small lake where transversal and second vertical modes are usually observed, *Limnol. Oceanogr.*, *42*, 663–673, doi:10.4319/lo.1997.42.4.0663.

Roget, E., I. Lozovatsky, X. Sanchez, and M. Figueroa (2006), Microstructure measurements in natural waters: Methodology and applications, *Prog. Oceanogr.*, *70*, 126–148, doi:10.1016/j.pocean.2006.07.003.

Rohr, J. J., E. C. Itsweire, and C. W. Van Atta (1984), Mixing efficiency in stably stratified decaying turbulence, *Geophys. Astrophys. Fluid Dyn.*, *29*, 221–236, doi:10.1080/03091928408248190.

Rothschild, B. J., and T. R. Osborn (1988), Small-scale turbulence and plankton contact rates, *J. Plankton Res.*, *10*, 465–474, doi:10.1093/plankt/10.3.465.

Saggio, A., and J. Imberger (2001), Mixing and turbulent fluxes in the metalimnion of a stratified lake, *Limnol. Oceanogr.*, *46*, 392–409, doi:10.4319/lo.2001.46.2.0392.

Saiz, E., A. Calbet, and E. Broglio (2003), Effects of small-scale turbulence on coperpods: The case of *Oithona davisae*, *Limnol. Oceanogr.*, *48*, 1304–1311, doi:10.4319/lo.2003.48.3.1304.

Sanchez, X., and E. Roget (2007), Microstructure measurements and heat flux calculations of a triple-diffusive process in a lake within the diffusive layer convection regime, *J. Geophys. Res.*, *112*, C02012, doi:10.1029/2006JC003750.

Schernewski, G., V. Podsetchine, and T. Huttula (2005), Effects of the flow field on small scale phytoplankton patchiness, *Nord. Hydrol.*, *36*, 85–98.

Seuront, L., F. Schmitt, and Y. Lagadeuc (2001), Turbulence intermittency, small-scale phytoplankton patchiness and encounter rates in plankton: Where do we go from here?, *Deep Sea Res. Part I*, *48*, 1199–1215, doi:10.1016/S0967-0637(00)00089-3.

Sharples, J., C. M. Moore, T. P. Rippeth, P. M. Holligan, D. J. Hydes, N. R. Fisher, and J. H. Simpson (2001), Phytoplankton distribution and survival in the thermocline, *Limnol. Oceanogr.*, *46*, 486–496.

Shimeta, J., P. A. Jumars, and E. J. Lessard (1995), Influences of turbulence on suspension feeding by planktonic protozoa; experiments in laminar shear fields, *Limnol. Oceanogr.*, *40*, 845–859, doi:10.4319/lo.1995.40.5.0845.

Slinn, D. N., and J. J. Riley (1996), Turbulent mixing in the oceanic boundary layer caused by internal wave reflection from sloping terrain, *Dyn. Atmos. Oceans*, *24*, 51–62, doi:10.1016/0377-0265(95)00425-4.

Smaoui, H., F. Boughanim, and G. Chapalain (2007), 1-D vertical model for suspended sediment transport in turbulent tidal flow: Application to the English Channel, *Comput. Geosci.*, *33*, 1111–1129, doi:10.1016/j.cageo.2006.11.016.

Smyth, W. D., and J. N. Moum (2000), Length scales of turbulence in stably stratified mixing layers, *Phys. Fluids*, *12*, 1327–1342, doi:10.1063/1.870385.

Smyth, W. D., J. N. Moum, and D. R. Caldwell (2001), The efficiency of mixing in turbulent patches: Inferences from direct numerical simulations and microstructure observations, *J. Phys. Oceanogr.*, *31*, 1969–1992, doi:10.1175/1520-0485(2001)031<1969:TEOMIT>2.0.CO;2.

Stansfield, K., C. Garrett, and R. Dewey (2001), The probability distribution of the Thorpe displacement within overturns in Juan de Fuca Strait, *J. Phys. Oceanogr.*, *31*, 3421–3434, doi:10.1175/1520-0485(2001)031<3421:TPDOTT>2.0.CO;2.

Staquet, C., and P. Bouruet-Aubertot (2001), Mixing in weakly turbulent stably stratified flows, *Dyn. Atmos. Oceans*, *34*, 81–102, doi:10.1016/S0377-0265(01)00062-8.

Sullivan, J. M., and E. Swift (2003), Effects of small-scale turbulence on net growth rate and size of ten species of marine dinoflagellates, *J. Phycol.*, *39*, 83–94, doi:10.1046/j.1529-8817.2003.02094.x.

Thorpe, S. A. (1977), Turbulence and mixing in a Scottish loch, *Philos. Trans. R. Soc. London Ser. A*, *286*, 125–181.

Thorpe, S. A. (2005), *The Turbulent Ocean*, Cambridge Univ. Press, Cambridge, U. K.

Timmermans, M. L., C. Garrett, and E. Carmack (2003), The thermohaline structure and evolution of the deep waters in the Canada Basin, Arctic Ocean, *Deep Sea Res. Part I*, *50*, 1305–1321, doi:10.1016/S0967-0637(03)00125-0.

Wang, Y., K. Hutter, and E. Bäuerle (2000), Wind-induced baroclinic response of Lake Constance, *Ann. Geophys.*, *18*, 1488–1501, doi:10.1007/s00585-000-1488-6.

Weibull, W. (1951), A statistical distribution function of wide applicability, *J. Appl. Mech.*, *18*, 293–297.

Wu, J. (1994), Altimeter wind and wind-stress algorithms: Further refinement and validation, *J. Atmos. Oceanic Technol.*, *11*, 210–215, doi:10.1175/1520-0426(1994)011<0210:AWAWSA>2.0.CO;2.

Wüest, A., and A. Lorke (2003), Small-scale hydrodynamics in lakes, *Annu. Rev. Fluid Mech.*, *35*, 373–412, doi:10.1146/annurev.fluid.35.101101.161220.

Wüest, A., D. C. Van Senden, J. Imberger, G. Priepke, and M. Gloor (1996), Comparison of diapycnal diffusivity measured by tracer and microstructure techniques, *Dyn. Atmos. Oceans*, *24*, 27–39, doi:10.1016/0377-0265(95)00408-4.

Wüest, A., G. Priepke, and D. C. Van Senden (2000), Turbulent kinetic energy balance as a tool for estimating vertical diffusivity in wind-forced stratified waters, *Limnol. Oceanogr.*, *45*, 1388–1400, doi:10.4319/lo.2000.45.6.1388.

Yamazaki, H., and D. Kamykowski (1991), The vertical trajectories of motile phytoplankton in a wind-mixed water column, *Deep Sea Res. Part A*, *38*, 219–241, doi:10.1016/0198-0149(91)90081-P.

Yamazaki, H., and R. Lueck (1987), Turbulence in the California Undercurrent, *J. Phys. Oceanogr.*, *17*, 1378–1396, doi:10.1175/1520-0485(1987)017<1378:TITCU>2.0.CO;2.

I. Lozovatsky, Environmental Fluid Dynamics Laboratories, Department of Civil Engineering and Geological Sciences, University of Notre Dame, Notre Dame, IN 46556, USA.

J. Planella Morato and E. Roget, Department of Physics, University of Girona, Campus de Montilivi, E-17071 Girona, Catalonia, Spain. (elena.roget@udg.edu)